"THERMAL PERFORMANCE ANALYSIS OF VARIOUS GAS FILLED SOLAR FLAT PLATE COLLECTORS"

A DISSERTATION

SUBMITTED IN PARTIAL FULFILLMENT OF THE REQUIREMENTS FOR THE AWARD OF THE DEGREE OF

MASTER OF TECHNOLOGY

IN

THERMAL ENGINEERING

Submitted by:

RAJAT KUMAR MISHRA

(Roll No. 2K17/THE/12)

Under the supervision of

PROF. AMIT PAL

And

DR. ANIL KUMAR

DEPARTMENT OF MECHANICAL ENGINEERING

DELHI TECHNOLOGICAL UNIVERSITY

(Formerly Delhi College of Engineering)

Bawana Road, Delhi-110042

JUNE, 2019

DELHI TECHNOLOGICAL UNIVERSITY

(Formerly Delhi College of Engineering)

Bawana Road, Delhi-110042

CANDIDATE'S DECLARATION

I, RAJAT KUMAR MISHRA, Roll No. 2K17/THE/12 student of M.Tech (Thermal Engineering), hereby declare that the project Dissertation titled "THERMAL PERFORMANCE ANALYSIS OF VARIOUS GAS FILLED SOLAR FLAT PLATE COLLECTORS" which is submitted by me to the Department of Mechanical Engineering, Delhi Technological University, Delhi in partial fulfillment of the requirement for the award of the degree of Master of Technology, is original and not copied from any source without proper citation. This work has not previously formed the basis for the award of any Degree, Diploma Associateship, Fellowship or other similar title or recognition.

Place: Delhi **RAJAT KUMAR MISHRA**

Date:

DEPARTMENT OF MECHANICAL ENGINEERING

DELHI TECHNOLOGICAL UNIVERSITY

(Formerly Delhi College of Engineering)

Bawana Road, Delhi-110042

CERTIFICATE

It is certified that the Project Dissertation titled "THERMAL PERFORMANCE ANALYSIS OF VARIOUS GAS FILLED SOLAR FLAT PLATE COLLECTORS" which is being submitted by RAJAT KUMAR MISHRA, Roll No. 2K17/THE/12, Department of Mechanical Engineering, Delhi Technological University, Delhi in partial fulfillment of the requirement for the award of degree of Master of Technology, is a record of the project work carried out by the student under our supervision. To the best of our knowledge this work has not been submitted in part or full for any Degree or Diploma to this University or elsewhere.

(DR. ANIL KUMAR)	**(DR. AMIT PAL)**
SUPERVISOR	**SUPERVISOR**
ASSOCIATE PROFESSOR	**PROFESSOR**

Place: Delhi

Date:

ACKNOWLEDGEMENT

Any accomplishment is a result of positivity of thoughts and efforts. It is important here to appreciate contribution, encouragement and support from persons who stood as 'Light House' throughout the voyage.

I take great pride in expressing my unfeigned appreciation and gratitude to my learned mentors Prof. Amit Pal and Dr. Anil Kumar, Department of Mechanical Engineering, Delhi Technological University, Delhi for their invaluable inspiration, guidance and continuous encouragement throughout this project work. Working under their guidance has been a privilege and an excellent learning experience that I will cherish for a long time.

I also appreciate and acknowledge the efforts of all those who have, directly or indirectly, helped me achieving my aim.

RAJAT KUMAR MISHRA

(Roll No. 2K17/THE/12)

M.Tech (Thermal Engineering)

Delhi Technological University, Delhi, India

ABSTRACT

The fossil fuels are depleting day by day and energy demand is rising at a high rate. The gap between this depletion and demand can be narrowed by the use of solar energy. The most direct application of solar energy is the conversion of solar radiation into thermal energy like in water heating system which is generally done using flat plate solar collectors. This research focuses on the media between the absorber plate and the glass cover. This study presents the performance evaluation of different gas filled solar flat plate collectors filled with gases like carbon dioxide, methane, nitrous oxide, R410a, sulphur hexafluoride, R22 and R134a to make greenhouse environment inside collector Their performances have been compared with the air filled solar flat plate collector. The complete analysis has been done for four different months (January, June, August, and October) under composite climatic condition of Delhi using MATLAB. The performance characteristic curves and equations for all gas filled collectors have been developed under clear sky condition.

The results show that there is 5.6, 2.8 and 2.3% decrease in average overall heat loss coefficient for carbon dioxide, nitrous oxide and R22 filled solar flat plate collector respectively as compared to air filled solar flat plate collector under clear sky condition. The average instantaneous efficiency has increased about 0.9% for carbon dioxide filled solar flat collector and 0.41% for both nitrous oxide and R22 filled solar flat plate collectors. Other filled gas solar flat plate collectors have lower performance than air filled solar flat plate collector. The average convective heat transfer coefficient between the absorber plate and glass cover decreases about 10.43% for carbon dioxide filled solar flat plate collector, 5.05% for nitrous oxide filled solar flat plate collector and 4.71% for R22 filled solar flat plate collector as compared to air filled solar flat plate collector.

The characteristic curve shows that the performance of carbon dioxide filled solar flat plate collector become better and better at higher water inlet temperature.

Thus, the carbon dioxide filled solar flat plate collector can be marked as the best among all these solar flat plate collectors. The MATLAB code that has been developed in this research can be used to analyze any gas filled solar flat plate collector.

TABLE OF CONTENTS

LIST OF FIGURES

LIST OF TABLE

NOMENCLATURE

δ	Declination angle
n	Number of days
θ	Angle of incidence for beam radiation
$\emptyset$	Latitude angle
γ	Surface azimuth angle
β	Slope of the inclined collector
ω	Hour angle
E	Equation of time correction (in minutes)
θ_z	Zenith angle
r_b	Tilt factor for beam radiation
r_d	Tilt factor for diffuse radiation
r_r	Tilt factor for reflected radiation
ρ	Reflectivity of surrounding surface
I_t	Flux falling on tilted surface at any instance (W/m^2)
I_b	Beam radiation (W/m^2)
I_d	Diffuse radiation (W/m^2)
Q_u	The rate of heat transfer to the work fluid (W)
A_p	Area of absorber plate (m^2)
S	Incident solar flux absorbed in the absorber plate (W/m^2)
Q_l	Rate of heat loss from top, bottom and sides (W)
α	Absorptivity of the absorber plate

$(\tau\alpha)_b$	Transmissivity-absorptivity product for beam radiation
$(\tau\alpha)_d$	Transmissivity-absorptivity product for diffuse radiation
η	Instantaneous collector efficiency
A_c	Collector gross area (area of the topmost cover including frame) (m^2)
θ_1	Angle of refraction for beam radiation
μ	Refractive index of glass
θ_2	Angle of refraction for diffuse radiation
ρ_{Ib} and ρ_{IIb}	Reflectivities of two components of polarization for beam radiation
τ_{rIb} andτ_{rIIb}	Transmissivities of two components of polarization for beam radiation
τ_{rb}	Transmissivity for beam radiation
τ_{ab}	Transmissivity based on absorption for beam radiation
k_g	Extinction coefficient of glass (m^{-1})
d_c	Thickness of the glass cover (m)
τ_b	Transmissivity of the cover system in case of beam radiation
ρ_{Id} and ρ_{IId}	Reflectivities of two components of polarization for diffuse radiation
τ_{rId} and τ_{rIId}	Transmissivities of two component of polarization for diffuse radiation
τ_{rd}	Transmissivity for diffuse radiation
τ_{ad}	Transmissivity based on absorption for diffuses radiation
τ_d	Transmissivity of the cover system in case of diffuse radiation
ρ_d	Diffuse reflectivity of the cover system
U_l	Overall heat loss coefficient (W/m^2-K)
T_{pm}	Average temperature of the absorber plate in Kelvin (K)

T_c	Glass cover temperature in Kelvin (K)
T_a	Temperature of the surrounding air (°C)
Q_t	Rate of heat loss from the top (W)
Q_b	Rate of heat loss from the bottom (W)
Q_s	Rate of heat loss from the sides (W)
U_t	Top loss coefficient (W/m^2-K)
U_b	Bottom loss coefficient (W/m^2-K)
k_i	Thermal conductivity of the back insulation (W/m-K)
δ_b	Thickness of the back insulation (m)
U_s	Side loss coefficient (W/m^2-K)
ε_p	Emissivity of absorber plate
ε_c	Emissivity of glass cover
h_{p-c}	Heat transfer coefficient between the absorber plate and glass cover
Nu_L	Nusselt number
Ra_L	Rayleigh number
k	Thermal conductivity of gas (W/m-K)
beta	Coefficient of volume expansion of gas (K^{-1})
Pr	Prandtl number of the gas filled inside the spacing
L	Spacing between the absorber plate and glass cover (m)
ν	Kinematic viscosity of the gas filled inside the spacing (m^2/sec)
h_w	Convective heat transfer coefficient at the top cover (W/m^2-K)
V_∞	Wind speed (m/s)

T_{sky}	Effective temperature of the sky (K)
K_P	Thermal conductivity of plate material (W/m-K)
δ_p	Plate thickness (m)
D_o	Outer diameter of tube (m)
W	Tube centre to centre distance (m)
ϕ	Plate effectiveness
D_i	Inner diameter of tube (m)
h_f	Fluid to tube heat transfer coefficient (W/m^2-K)
F	Collector efficiency factor
F_R	Collector heat removal factor
$\dot{m}$	Mass flow rate of water in tube (kg/s)
C_p	Specific heat capacity of water (J/kg-K)
T_{fo}	Water Outlet temperature of water (^oC)
T_{fi}	Water Inlet temperature of water (^oC)

CHAPTER 1

INTRODUCTION

1.1 The rising demand for energy

Energy is one of the important inputs that add on to the economic development of any country. It is predicted that global demand for energy will increase in the upcoming years. The energy needs are predicted to expand by 55% from 2005 to 2030, with hike from 11.4 to 17.7 billion tonnes of oil equivalent. The energy consumption is expected to increase by 50% due to bulk of demand coming from developing countries. Oil, coal and gas majorly account for the primary energy consumption. The renewable energy accounted for 8.3% of final energy consumption in the UK in 2015. The world population is increasing at a rapid rate and is predicted to increase by 1 billion by next ten years and reach 9.6 billion by 2050. Huge amount of energy is consumed by the developed countries and the demand is increasing in developing countries due to growing population and increasing standard of people [1].

1.2 Global reserve and estimated life of commercial energy sources

The commercial energy is obtained mainly from the three kinds of fuel: coal, oil and natural gas. According to BP Statistical Review of World Energy, the total global reserves of fossil fuel are Coal - 1,139 billion tonnes, Natural Gas -187 trillion cubic meters, Crude Oil - 1,707 billion barrels. These volumes may seem large at a glance but these conventional fossil fuels are exhaustible. They cannot meet up the increasing energy demand in future. These fossil fuels would be exhausted as follows: [2]

Coal - year 2169

Natural Gas - year 2068

Crude Oil - year 2066

1.3 Solar as an option

The population and demand of energy is increasing at very fast rate. This has led to the need of alternative energy source and solar energy is a very good option. Solar energy is infinite and a lot of things can run using solar power with less maintenance. 174 peta watts of energy hit our atmosphere in the form of solar radiation but one third of this is reflected back into space. The atmosphere, clouds, oceans and land absorb 3850000 exajoules every year. The solar energy that hits the Earth every second is equivalent to 4 trillion 100-watt light bulbs. The world's energy consumption for an entire year can be fulfilled just by one hour of solar radiation [3]. There are two ways in which solar energy can be utilized. First is solar electric and other is solar thermal. Solar electric constitutes of photovoltaic system that directly converts sunlight into electricity using panels made of semiconductor cells. There are several problems with photovoltaic solar energy because of its low efficiency and high cost. The solar thermal technology uses the sunrays directly by producing heat. They use solar collector for this purpose. It is a device that absorbs the solar radiation and converts it into heat and transfers this heat to a fluid through the collector [4]. The potential of solar energy can be effectively utilized in developing smart cities (Mishra et al., 2019) (Appendix 4).

1.4 Types of Solar Collectors

1.4.1 Flat Plate Collector-

As shown in Fig.1.1, the solar radiation strikes the transparent glass cover (glazing sheet) and passes on the blackened high absorptivity absorber plate. This plate absorbs large portion of this energy and it is then transferred to the transport medium in the fluid tubes. The medium is further utilized for storage or use. The liquid tubes are welded to the absorbing plate and are connected at both ends by large diameters header tubes.

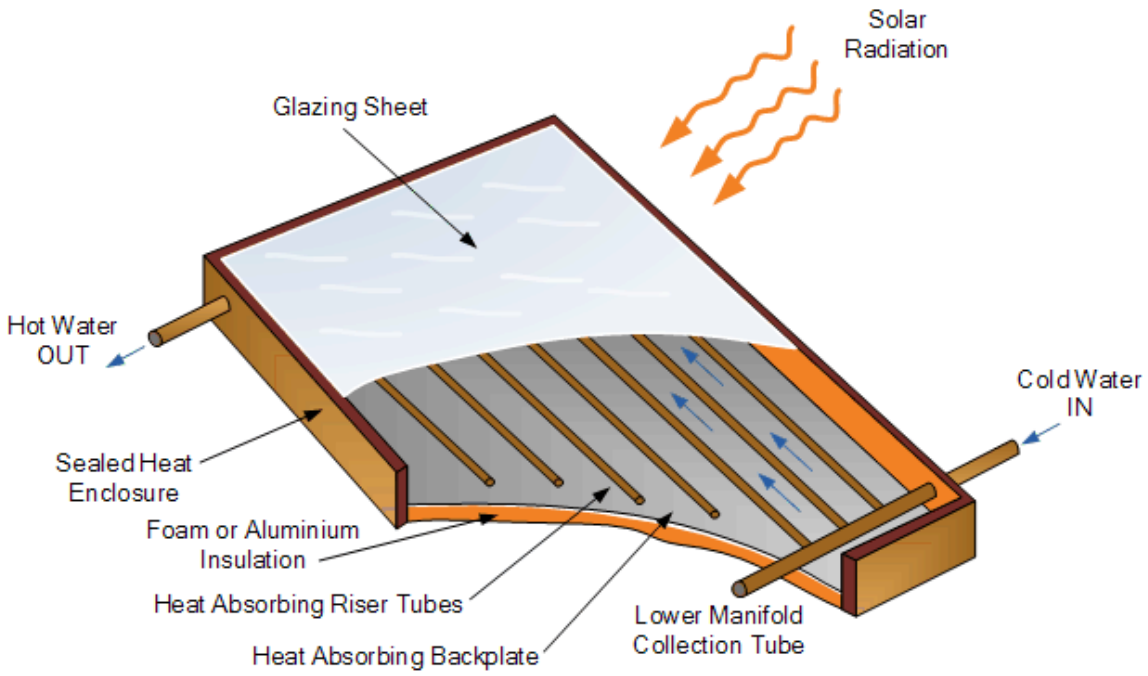

Fig.1.1 Schematic representation of Solar Flat Plate collector [5]

The transparent glass cover reduces the convection losses between the absorber plate and the glass radiation losses from the collector. The glass is transparent to the short-wave radiation that is received by the sun but it is almost opaque to long-wave thermal radiation emitted by the absorber plate. This makes greenhouse effect inside the space between the absorber tube glass cover.

These flat plate collectors are usually stationary and have no tracking of the sun. The orientation of these collectors should towards the equator. It should face south in the northern hemisphere and north in the southern hemisphere [4].

All the materials used in the collector should be able to withstand high temperatures up to 200°C. The absorber plate is made up of metallic materials like copper, steel or aluminum. The housing material of the collector can be of plastic, metal or wood. The back and side insulation are done to reduce the heat losses. The absorber sheet is made of high thermal conductivity and high absorptivity for short-wavelength radiations. The flat-plate collector unlike concentrating collectors utilizes both beam and diffuse solar radiation for various applications [6].

1.4.2 Evacuated tube collector

As shown in Fig. 1.2 evacuated tube collectors consist of two concentric glass tubes. The annular space between both glass and tube is evacuated. There is selective coating on the outer surface of the inner glass tube. This outer surface absorbs the solar radiation and some part of this radiation goes through conduction through the wall of tube. The inner tube is filled with water. Thermosyphon action causes the heat transfer action. The convection heat loss reduces due to vacuum in the annular space [7].

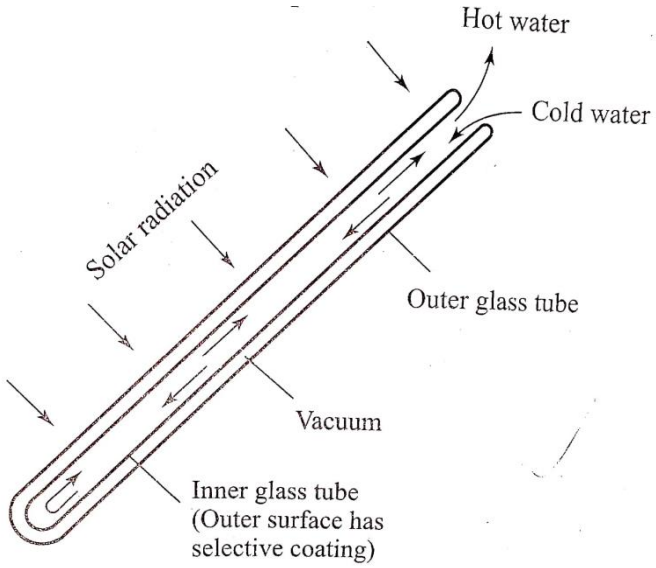

Fig. 1.2 Schematic representation of an evacuated tube collector module [7]

1.4.3 Cylindrical parabolic concentrating collector

Fig 1.3 shows a linear parabolic-shaped reflector. It focuses the sun's radiation onto a linear receiver tube that is located along focal line of parabolic trough collectors. The collector has the tracking system so that the sun is continuously focused on the receiver.

The system has single axis tracking system. It can be mechanical and automatic both.

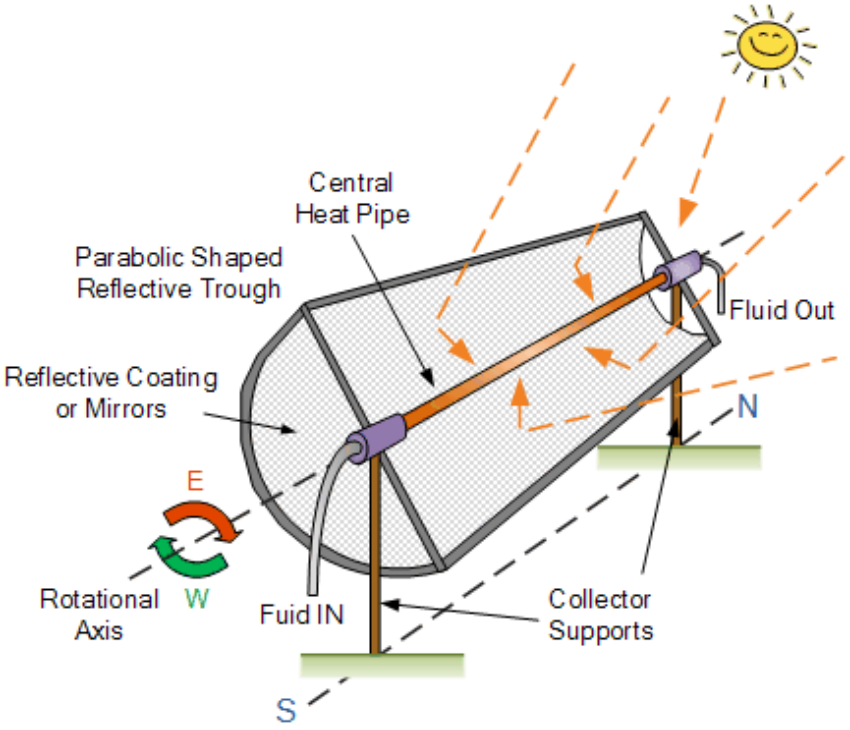

Fig 1.3 Schematic diagram of cylindrical parabolic concentrating collector [8]

In tracking system, the troughs get slowly rotated by the mechanical drives during the day so that the reflected sunlight is focused onto the pipe receivers. The fluid flowing in the tube can be heated up to 400°C [9]. This working fluid is utilized in generating high-pressure superheated steam which then fed to a conventional steam turbine to produce electricity.

1.4.4 Parabolic dish collector

Fig.1.4 shows a parabolic dish collector in which a point focus collector that tracks the sun in two axes. It focuses the solar energy onto a receiver located at the focal point of the dish. Two axis tracking system is employed in this system. The receiver of the collector absorbs the radiant solar energy and converts it into thermal energy that goes into the circulating fluid. If engine-generator is coupled directly to the receiver then this thermal energy can be converted into electricity. This system can achieve temperatures in excess of 1500°C [4].

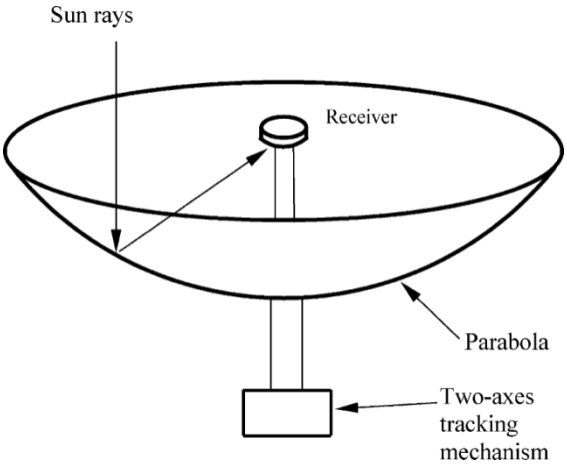

Fig.1.4 Schematic representation of parabolic dish collector [4]

1.4.5 Heliostat field collector

Fig.1.5 shows heliostat field or central receiver collector. A number of tracking flat mirrors or heliostats are mounted with some slightly concave mirror segments on the heliostats directs the solar energy to the single receiver which further get transferred to the circulating fluid that can be stored or can be used to generate electricity. This system is highly efficient both in collecting energy and in converting it to electricity [10].

The average solar flux that impinges on the receiver varies between 200 and 1000 kW/m^2. Thus, the high flux allows working temperatures is more than 1500 ºC [4].

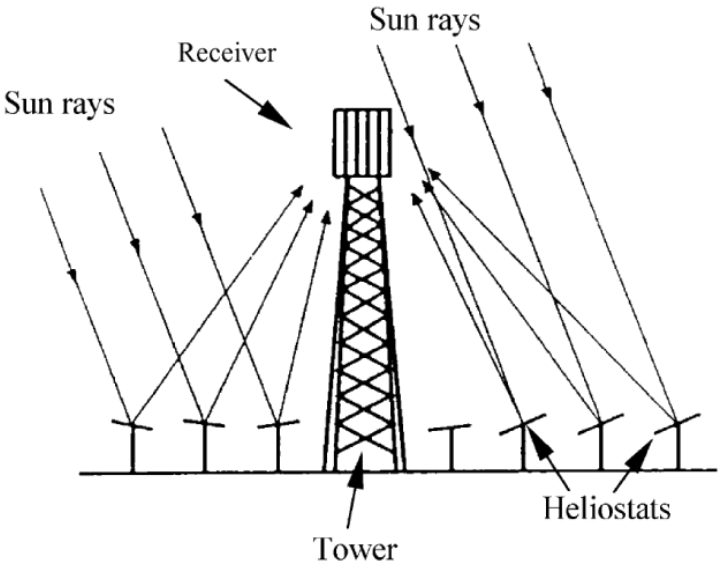

Fig.1.5 Schematic of central receiver system [4]

In all above-mentioned collectors, flat plate collectors and evacuated tube collector are used most widespread. There are various applications of both flat plate collectors and

evacuated tube collectors such as solar water heating systems, solar refrigeration, solar space heating and cooling, solar distillation, solar drying and industrial process heat. Hence in this study flat plate collectors are analyzed.

1.5 Solar radiation at the Earth's surface and Greenhouse effect

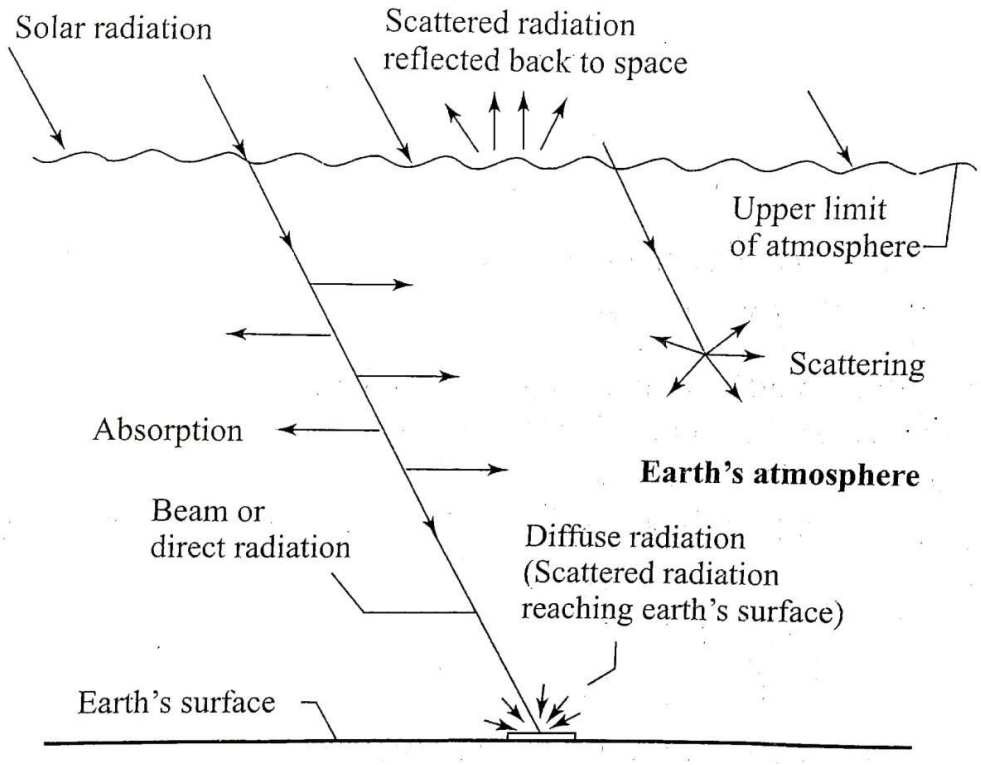

Fig.1.6 Schematic representation of absorption, scattering, beam & diffuse radiation [7]

Solar radiation that is received at the earth's surface goes through various mechanisms. As shown in the Fig.1.6 radiation reaches the atmosphere, some part of it get absorbed the gases present in the atmosphere. This absorption is due to gases like carbon dioxide, ozone, methane, water vapor etc. The presence of these gases and particulate matter causes scattering of some part of these solar radiations. This scattered part is redistributed in all direction. Some part goes back to space and some reaches the earth's surface as diffuse radiation. Solar radiation that reaches directly to the earth's surface is called as direct or beam radiation. The sum of direct and diffuse radiation is total radiation [7].

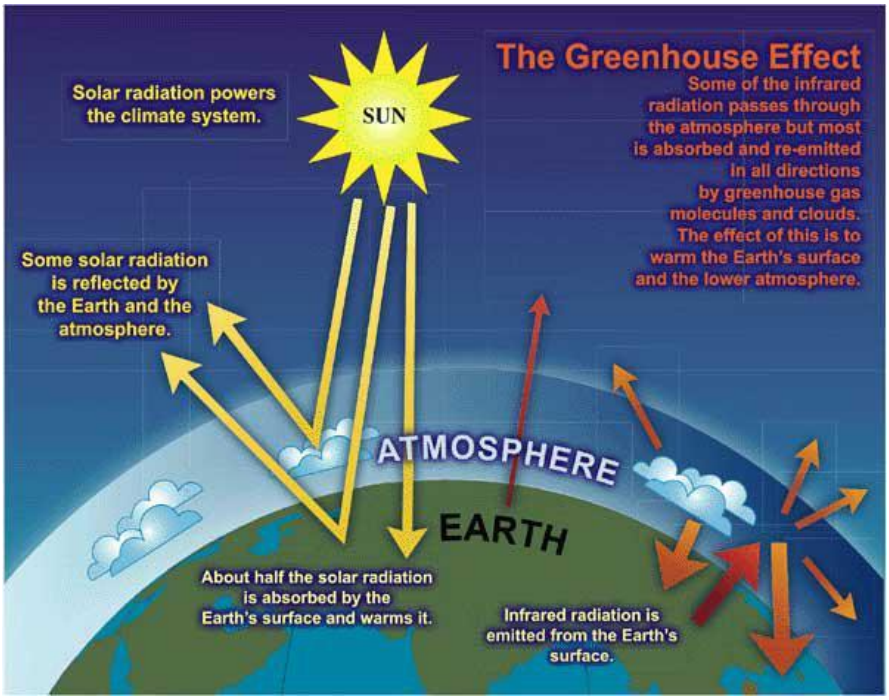

Fig.1.7 Pictorial representation of Greenhouse mechanism [11]

Fig.1.7 shows the greenhouse mechanism. The earth's surface gets warmed during the day and cools down in the night. The warmed earth emits radiation upwards. If there had been no atmosphere, then this upward radiation going from the earth in night would balance the incoming energy absorbed from the sun. The mean surface temperature of earth would have been around -18°C, 33°C colder than the observed mean surface temperature. Therefore, presence of some greenhouse gases in the atmosphere is needed. Infrared radiations (long wavelengths) are emitted by the earth in night and are strongly absorbed by the greenhouse gases in the atmosphere, such as water vapor, carbon dioxide and methane and warm the atmosphere. Hence, the surface temperature of the globe is around 15°C on average. This is called as natural greenhouse effect. If greenhouse gases are increased in the atmosphere say from human activities, then more amounts infrared radiations will be absorbed. This is called as enhanced greenhouse effect [11].

1.6 Organization of the Dissertation

Chapter 1 discusses the rising demand for energy in current scenario and describes solar energy as an alternative option to fossil fuels. It also discusses various kinds of solar collectors and mechanism of solar radiation and greenhouse effect on Earth.

Chapter 2 deals with the literatures related to the media between the absorber and the glass cover in solar collectors. It also highlights the research gap and objectives of this research.

Chapter 3 focuses on the methodology that has been used in this research work. All the input parameters, process and calculations that has been done in MATLAB are discussed.

Chapter 4 presents the discussions on findings/results.

Chapter 5 highlights the conclusions and future scope of this conducted research.

References

Appendices

CHAPTER 2

LITERATURE REVIEW

This chapter deals with the literatures related to the media between the absorber and glass cover in solar collectors. It also discusses the research gap and objectives of this research.

2.1 Literature Survey

Makhanlall and Jiang [12] conducted the performance analysis and optimization of a vapor-filled flat-plate solar collector. The research showed thermodynamic analysis of flat plate solar collector in which water vapor replaces the air between the glass cover and absorber plate. The analysis of the influence of solar irradiation, inclination angle, as well as the use of absorbers with different emissivity values had been done. It had been carried out with the computational fluid dynamics (CFD) code FLUENT 6.3. Entropy generation due to natural convection-radiation interaction in an enclosure filled with water vapor was taken in the model. The vapor acted as an absorbing, emitting and scattering gas.

The research showed the variation of absorber mean temperature, thermal losses and entropy generation number of the vapor-filled collector with the irradiation ranging 500 to 1200 $W/m^{2.}$ The convective and radiative heat losses increased as the temperature difference over the vapor layer increased. The entropy generation number also followed the same trend with the irradiance. The radiation entropy generation number was larger than the convection entropy generation number at a high irradiation flux. At a low irradiation flux, however, both entropy generation numbers almost had same value.

The absorber mean temperature, thermal losses, and entropy generation number all increased as absorber emissivity decreased. The low emissivity cover and high emissivity absorber gave best combination. For the high emissivity absorber plate, the

radiation entropy generation number is larger than the conduction entropy generation number but vice versa for the low emissivity absorber plate.

The optimum angle of inclination was found approximately equal to the latitude of the location. The absorber mean temperature, thermal losses, and entropy generation number were minimum at zero-degree angle of inclination. This was different than air filled solar flat plate collectors that show their best performance at a high degree of inclination. Convection entropy generation number was not significantly affected by inclination but the radiation entropy generation number increased.

The performance of vapor-filled flat-plate solar collector improved if irradiation intensity, inclination angle and glass cover emissivity is low and absorber emissivity is high.

Moss et al. [13] studied and analyzed the evacuated flat plate solar collector. Two collectors were built for the analysis. First had metal tray to the rear and second one used two glass sheets. An array of pillars was there to support the glass against atmospheric pressure. Cerasolzer 217, a low temperature solder was used there. It had been applied using ultrasonic iron. Some resealing was also done with epoxy resin due to thermal stresses during vacuum creation in solar collectors.

Both the collectors showed decrease in heat loss coefficient and increase in efficiency compared to convention solar flat plate collectors if they are evacuated below 0.5 Pa. The heat loss coefficient went from 7.4 to 3.6 W/m^2K. However, the efficiency of these tested collectors was found to be lower than non-evacuated commercial collectors as the black chrome coating used there had high emissivity. The simulation said that if higher quality coating is used then the efficiency increases significantly than the conventional flat plate solar collectors. The research described that if irradiance is less than 500 W/m^2 then there is significant increase in efficiency of evacuated flat plate collectors than conventional one.

Vestlund et al. [14] analyzed the gas filled solar flat plate collector in which the space between the absorber and the glass plate was filled with some inert gases like xenon (Xe), and it was possible to reduce the influence of humidity condensate and dust. The research was analyzed on a model made on MATLAB with standard heat transfer formulas. It said that as d_{pg} (distance between the absorber plate and glass cover) rises,

the edge loss also increases. The model used $U = \frac{q}{(Tw-Ta)}$ for U value (overall loss coefficient). Tw and Ta were the mean heat transfer medium temperature and ambient temperature respectively. The research discussed the influence of the distance between absorber and glass (d_{pg}) and the different collector components on overall U-value.

The influence of other gases like air, xenon, carbon dioxide and argon on overall heart loss had also been studied. The best alternative was xenon gas as it reduced the overall heat loss coefficient by about 20%. The thin collector filled with inert gas has lower loss compared to conventional air filled solar flat plate collectors.

Makhanlall et al. [15] discussed about the entropy generation in a solar collector filled with a radiative participating gas. The losses in collectors are due to thermodynamic irreversibility that causes entropy generation. These losses could be reduced through EGM (entropy generation minimization) techniques.CFD had been used to study the dissipation, heat conduction and convection, and thermal radiation of solar collector filled with a radiative participating gas. Thermal efficiency of the best solar collectors could reach up to 80%. Thus, enhancing the efficiency using energy conservation techniques i.e. 1st law only has lower margin. Hence 2nd law of thermodynamics, and its design related concept of EGM could be utilized for further performance optimization of these solar collectors. Entropy generation in gas layer of solar collectors is associated with combined convection and radiation heat transfer. Its analysis requires considerable computational effort because of the integral-differential nature of the gas radiation equations.

The entropy generation due to combined convection and radiation heat transfer in a flat plate solar collector filled with carbon dioxide gas had been studied. It had been assumed that the working fluid emits, absorbs and anisotropically scatters thermal radiation. Natural flow of the water vapor was taken in the model of flat plate collector. The study was limited to Rayleigh number smaller than 5×10^4. Therefore, 2D laminar flow can be assumed to exist. The rate of entropy generation in the gas layer was found to be approximately 0.002 W/K. Conduction and convection caused 60% of the total entropy generation, 39% due to radiative heat transfer processes and 1% in the gas. There is an optimum optical thickness and an optimum tilt angle where the heat losses are minimum, radiative entropy generation should be considered in natural convection processes in these gasses filled solar collectors. The transfer processes at the solid

boundaries causes radiative entropy generation and solar collectors filled with a radiative participating gas are suitable for the tropics.

Sadeghi et al. [16] performed a comparative study of air and argon gases between cover and absorber coil in a cylindrical solar water heater (CSWH). Argon gas had been used between the cover and the absorber of the CSWH. The effect of the gas between the cover and the absorber at various mass flow rates had been studied in this research. Argon filled cylindrical solar water heater had been compared with the air filled cylindrical solar water heater. Four different mass flow rates of 2.5, 3, 3.5 and 4 kg/h had been used in the analysis to get the optimum mass flow rate corresponding to maximum energy efficiency. It had been seen that as the mass flow rate increases from 2.5 to 4 kg/h, there is decrease in the temperature difference between the inlet and outlet of water due to reduction in residence time of it in the copper coil absorber. The maximum temperature difference was reported as 23°C for the argon gas at a mass flow rate of 2.5 kg/h, while the minimum temperature difference as 13°C for air at mass flow rate of 4 kg/h. The thermal efficiency of the proposed CSWH, using argon gas increases the energy efficiency of the collector up to about 4%. At an optimum mass flow rate of 3.5 kg/h, there was the highest energy efficiency value of 48.17 and 52.14% for the air and argon, respectively. The economic analysis said that constructing a cylindrical solar collector costs $150, whereas manufacturing a flat plate solar collector with similar efficiency costs $260 i.e. about 73% more.

Garcia et al. [17] conducted the experimental evaluation of solar flat plate collectors introducing convective barriers. The possible improvements in the thermal efficiency of solar flat plate collectors that are generally used in domestic heating had been done. The convective barriers were included between the absorber plate and glass cover. The experiment was done using up to four convective barriers and their results were compared with simple solar collector, without any convective barrier. Including different numbers of convective barriers do not change solar collector transparency i.e. radiation absorbing capacity as maximum thermal efficiency remains same. Three equally spaced barriers gave the lower global heat loss transfer. There was 5.25% reduction in global loss heat transfer coefficient. Each solar collector design requires an optimal number of convective barriers.

Nahar and Garg [18] discussed about the free convection and shading due to gap spacing between an absorber plate and the cover glazing in solar flat plate collector. In this the gap between the absorber plate and the glass cover had been optimized by considering convective losses as well as the shading of the absorber plate by the side walls for more efficient collection of solar radiation. There was a decrease in free convection heat transfer coefficient with increasing gap as if the gap was increased from 1 cm to 3, 4, 5 or 8cm; there was a reduction in convection losses of 11, 13, 14and 20% respectively. Correspondingly the area of the collector that had been shaded was 2.6, 3.4, 4.4 and 7% respectively. The gap of between 4 and 5cm should be maintained between the absorber and the cover glazing for minimum convection losses and minimum shading in solar energy flat plate collectors.

Buchberg et al. [19] studied the effect of spacing between the absorber and the cover. Calculations had been done involving single and double cover collector having non selective absorber plate and single cover collector having selective absorber plate. The both spacing had been tested under same operating conditions and efficiency for all of them was found. It was found that if the larger spacing i.e. around 5cm is used then area requirement for the collector can be reduced by 2 to 8%, higher reduction is for the collector with the selective absorber plate.

Beikircher et al. [20] performed an experimental investigation on the heat loss by the gas conduction of an evacuated solar flat plate collector. The research showed that the gas conduction gets completely reduced if evacuation is done below 0.1 Pa and total losses get halved. There is another method to reduce the gas conduction by substituting the air by other gases like xenon, krypton and argon at moderate pressure. The experiments carried out with air in pressure range of 10^{-3} to 10^{4} Pa and above 10 Pa for argon gas. The filled gases reduced the gas conduction up to 75%.

2.2 Research gap

Ongoing through the research works involving the study of gas filled solar collectors, it has been found that very limited work has been done regarding this kind of solar collectors. Also, there is little discussion regarding the influence of greenhouse gases in the space between absorber plate and glass cover if air is replaced by these gases. The performance of solar flat plate collector is expected to increase with insertion of greenhouse gases.

2.3 Objectives

Based on literature review and research gap identified, following are the objectives of this research.

- Performance evaluation of solar flat plate collector filled with different gases and their comparison with air filled solar flat plate collector under composite climatic condition of Delhi.

- Evaluation of overall heat loss coefficient and convective heat transfer coefficient between the absorber plate and glass cover for all gas filled solar flat plate collectors under clear sky condition.

- To develop performance characteristic curve and characteristic equation of all gas filled solar flat plate collectors under clear sky condition.

CHAPTER 3

METHODOLOGY

The performance evaluation of solar flat plate collector filled with different gases has been done for four different months of 2016 under four different climatic conditions. January, June, August and October have been chosen as these months have different climatic conditions in terms of solar radiation, velocity of the wind, ambient temperature and other factors [21].Different climatic conditions give different environment to collectors like the corresponding losses are different and thus this analysis of solar flat plate collector in these four months under the following climatic conditions helps in estimating its overall performance for the year.

A. Clear sky condition
B. Hazy day (fully)
C. Hazy and cloudy (partially)
D. Cloudy (fully)

Delhi has been chosen for the analysis as it has a composite climate. All the hourly radiation data and ambient temperature is taken from the data provided by the IMD Pune listed in the Appendix 1**.** The appendix 1 shows A, B, C and D according to the above-mentioned sequence.

The clear sky condition is seen on 15th January, 17th June, 16thAugust and 20thOctober. Hazy condition is seen on 17thJanuary, 16thJune, 18thAugust and 18thOctober. Hazy and cloudy condition is seen on 16thJanuary, 18thJune, 19th August and 17thOctober. The cloudy condition is seen on 18thJanuary, 20thJune, 20thAugust and 15thOctober.

3.1 Model of Gas filled solar flat plate collector

The model of the gas filled solar flat plate collector has been developed in solid works.

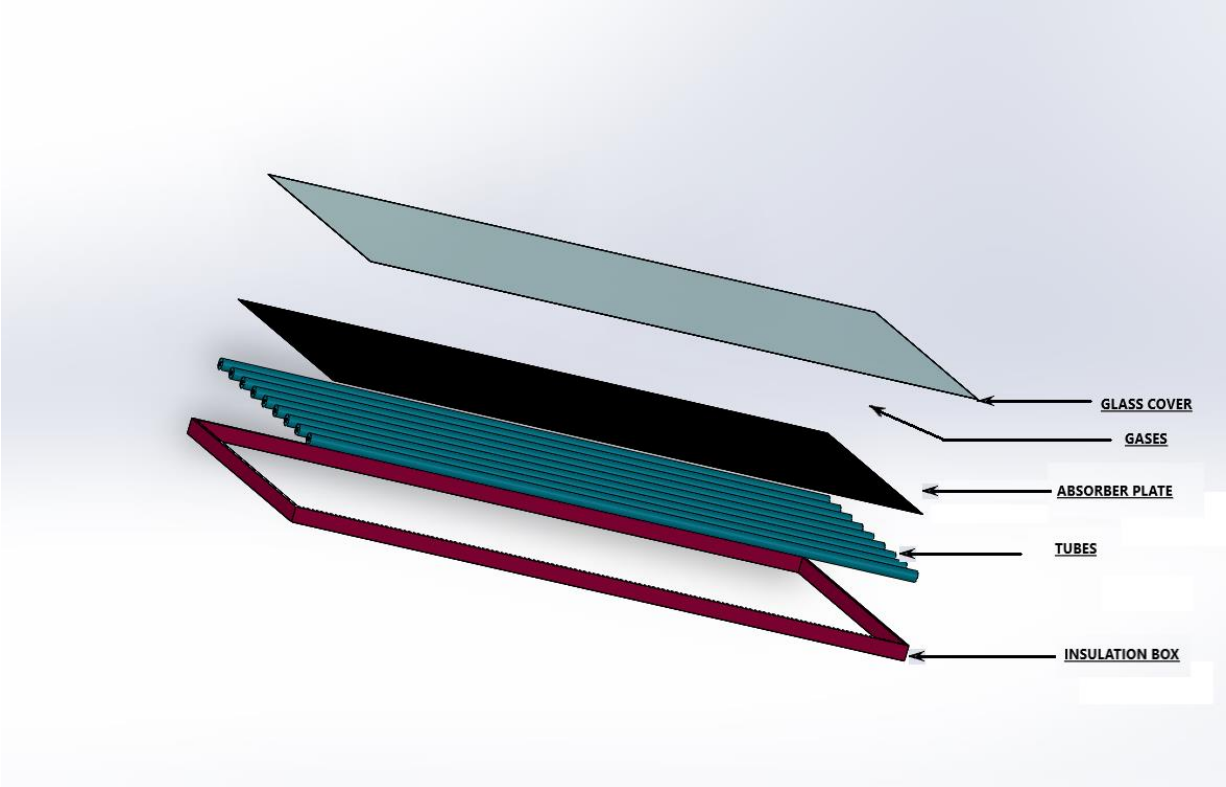

Fig.3.1 Model of gas filled solar flat plate collector

Fig.3.1 represents the model of gas filled solar flat plate collector. The space between the absorber plate and glass cover is filled with different gases. The tubes are fabricated below the absorber plate. Insulation setup is provided to the back side as insulation box.

3.2 Gases filled in Solar Flat Plate Collectors

Carbon dioxide, methane, nitrous oxide, R410a, sulphur hexafluoride, R22 and R134a have been chosen for the filling the inside space between the absorber plate and the glass cover. These gases have selected because of their considerable greenhouse potential and lower ozone depletion potential. Table 3.1 shows the global warming potential of these gases at 100-year time horizon.

Table 3.1 Global warming potential of different gases [22, 23]

Gases	**Global warming Potential (100 years' time horizon)**
Carbon dioxide (CO_2)	1
Methane (CH4)	21
Nitrous Oxide (N_2O)	310
R410a	2088
Sulphur hexafluoride	23900
R22	1810
R134a	1430

The ozone depletion potential (ODP) for all these gases is not much with maximum of 0.055 for R22.Other gases have either zero ODP or very low ODP values [23].

3.3 Performance evaluation of gas filled solar flat plate collector

3.3.1 Equations and correlations

Different equations and correlation which have been used in this analysis for determining various parameters of solar flat plate collectors are discussed below**.**

Cooper [24] gave the relation for declination angle.

$$\delta(\text{in degrees}) = 23.45\sin\left[\frac{360}{365}(284 + n)\right] \quad (3.1)$$

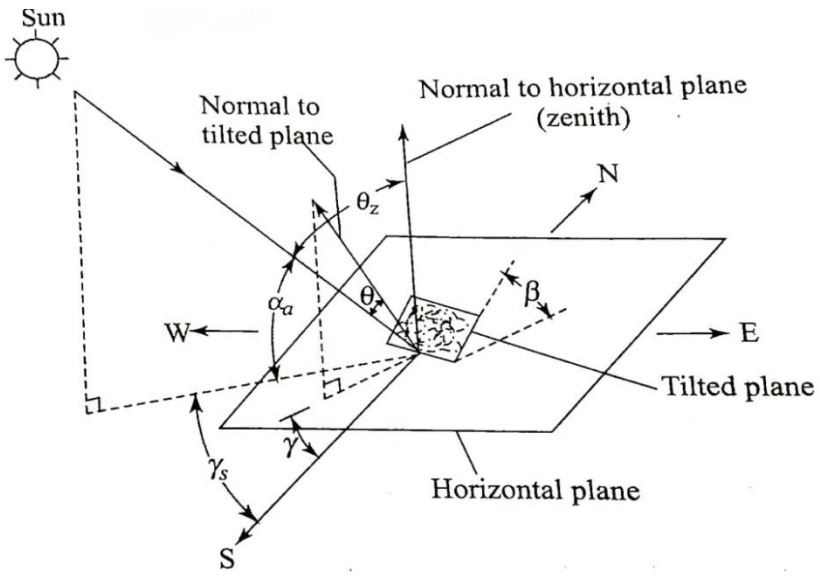

Fig.3.2 Solar radiation geometry [25]

Fig.3.4 shows different angles as the radiation strikes the horizontal surface and tilted surface.

The relations between the different angles are given.

$\cos\theta = \sin\emptyset(\sin\delta\cos\beta + \cos\delta\cos\gamma\cos\omega\sin\beta) + \cos\emptyset(\cos\delta\cos\omega\cos\beta - \sin\delta\cos\gamma\sin\beta) + (\cos\delta\sin\gamma\sin\omega\sin\beta)$ (3.2)

For vertical surface, $\beta = 90^0$

$$\cos\theta = \sin\emptyset\cos\delta\cos\gamma\cos\omega - \cos\emptyset\sin\delta\cos\gamma + \cos\delta\sin\gamma\sin\omega \quad (3.3)$$

For horizontal surface, $\beta = 0^0$

$$\cos\theta = \sin\emptyset\sin\delta + \cos\emptyset\cos\delta\cos\omega \quad (3.4)$$

For inclined surface facing due south $\gamma = 0^0$

$\cos\theta = \sin\emptyset(\sin\delta\cos\beta + \cos\delta\cos\omega\sin\beta) + \cos\emptyset(\cos\delta\cos\omega\cos\beta - \sin\delta\sin\beta)$

$= \sin\delta\sin(\emptyset - \beta) + \cos\delta\cos\omega\cos(\emptyset - \beta)$ (3.5)

Local apparent time (LAT) = Standard time ± 4(Standard time longitude – longitude of location) + (Equation of time correction) (3.6)

$$\omega = (720 - \text{LAT})\frac{15}{60} \quad (3.7)$$

The equation of time correction (in minutes) [26]

$$E = 229.18(0.000075 + 0.001868\ \cos B - 0.032077\ \sin B - 0.014615\ \cos 2B - 0.04089\ \sin 2B) \quad (3.8)$$

$$B = (n-1)\frac{360}{365} \quad (3.9)$$

$$r_b = \frac{\cos\theta}{\cos\theta z} = \frac{\sin\delta\sin(\emptyset-\beta)+\cos\delta\cos\omega\cos(\emptyset-\beta)}{\sin\emptyset\sin\delta+\cos\emptyset\cos\delta\cos\omega} \quad (3.10)$$

$$r_d = \frac{1+\cos\beta}{2} \quad (3.11)$$

$$r_r = \rho\frac{(1-\cos\beta)}{2} \quad (3.12)$$

$$I_t = I_b r_b + I_d r_d + (I_b + I_d) r_r \quad (3.13)$$

$$Q_u = A_p S - Q_l \quad (3.14)$$

$$\eta = \frac{\text{Useful heat gain}}{\text{Radiation incident on the collector}} = \frac{Q_u}{A_c I_t} \quad (3.15)$$

$$\theta_1 = \sin^{-1}\frac{(\sin\theta)}{\mu} \quad (3.16)$$

$$\rho_{Ib} = \frac{\sin^2(\theta_1-\theta)}{\sin^2(\theta_1+\theta)} \quad (3.17)$$

$$\rho_{IIb} = \frac{\tan^2(\theta_1-\theta)}{\tan^2(\theta_1+\theta)} \quad (3.18)$$

$$\tau_{rb} = \frac{1}{2}(\tau_{rIb} + \tau_{rIIb}) \quad (3.19)$$

$$\tau_{rIb} = \frac{1-\rho_{Ib}}{1+\rho_{Ib}} \quad (3.20)$$

$$\tau_{rIIb} = \frac{1-\rho_{IIb}}{1+\rho_{IIb}} \quad (3.21)$$

$$\tau_{ab} = e^{\frac{(-k g d_c)}{\cos\theta_1}} \quad (3.22)$$

$$\tau_b = \tau_{ab}\tau_{rb} \quad (3.23)$$

Angle of incidence for the diffuse radiation can be taken as 60° [7]

$$\theta_2 = \sin^{-1}\frac{(\sin 60)}{\mu} \quad (3.24)$$

$$\rho_{Id} = \frac{\sin^2(\theta_2 - 60)}{\sin^2(\theta_2 + 60)} \quad (3.25)$$

$$\rho_{IId} = \frac{\tan^2(\theta_2 - 60)}{\tan^2(\theta_2 + 60)} \quad (3.26)$$

$$\tau_{rId} = \frac{(1 - \rho_{Id})}{(1 + \rho_{Id})} \quad (3.27)$$

$$\tau_{rIId} = \frac{(1 - \rho_{IId})}{(1 + \rho_{IId})} \quad (3.28)$$

$$\tau_{rd} = \frac{(\tau_{rId} + \tau_{rIId})}{2} \quad (3.29)$$

$$\tau_{ad} = e^{\frac{(-k_g d_c)}{\cos\theta_2}} \quad (3.30)$$

$$\tau_d = \tau_{rd}\tau_{ad} \quad (3.31)$$

$$\rho_d = \tau_{ad} - \tau_d \quad (3.32)$$

$$(\tau\alpha)_b = \frac{(\tau_b \times \alpha)}{1 - (1 - \alpha)\rho_d} \quad (3.33)$$

$$(\tau\alpha)_d = \frac{(\tau_d \times \alpha)}{1 - (1 - \alpha)\rho_d} \quad (3.34)$$

$$S = I_b r_b (\tau\alpha)_b + \{I_d r_d + (I_b + I_d) r_r\} (\tau\alpha)_d \quad (3.35)$$

$$Q_l = U_l A_p (T_{pm} - T_a + 273.2) \quad (3.36)$$

$$U_b = \frac{k_i}{\delta_b} \quad (3.37)$$

$$U_s = 10\ \%\ \text{of}\ U_b \quad (3.38)$$

$$Q_l = Q_t + Q_b + Q_s \quad (3.39)$$

$$Q_t = U_t A_p (T_{pm} - T_a + 273.2) \quad (3.40)$$

$$Q_b = U_b A_p (T_{pm} - T_a + 273.2) \quad (3.41)$$

$$Q_s = U_s A_p (T_{pm} - T_a + 273.2) \quad (3.42)$$

Under steady state the heat transfer from the absorber plate to glass cover is equal to the heat transfer from glass cover to surroundings. It is assumed that there is system of

parallel surfaces in between the absorber plate and the glass cover and heat flow is steady and 1-D [27].

$$\frac{Q_t}{A_p} = h_{p-c}\left(T_{pm} - T_c\right) + \frac{5.67\times10^{-8}\left({T_{pm}}^4 - {T_c}^4\right)}{\left(\frac{1}{\varepsilon_p}+\frac{1}{\varepsilon_c}-1\right)} \quad (3.43)$$

$$Ra_L = \frac{9.81\times(beta)\times\left(T_{pm}-T_c\right)\times L^3\times Pr\times\cos\beta)}{\nu^2} \quad (3.44)$$

Buchberg et al. [19] suggested some correlations to find out the convective heat transfer coefficient between the absorber plate and glass cover.

$$Nu_L = 1;\ Ra_L\cos\beta < 1708 \quad (3.45)$$

$$Nu_L = 1 + 1.446\left(1 - \frac{1708}{Ra_L\cos\beta}\right);\ 1708 < Ra_L\cos\beta < 5900 \quad (3.46)$$

$$Nu_L = 0.229(Ra_L\cos\beta)^{0.252};\ 5900 < Ra_L\cos\beta < 9.23\times10^4 \quad (3.47)$$

$$Nu_L = 0.157(Ra_L\cos\beta)^{0.285};\ 9.23\times10^4 < Ra_L\cos\beta < 10^6 \quad (3.48)$$

Test et al. [28] gave heat transfer coefficient at the top cover

$$h_w = 8.55 + 2.56\,V_\infty \quad (3.49)$$

$$T_{sky} = T_a + 273.2 - 6 \quad (3.50)$$

$$m = \left(\frac{U_l}{K_P x\,\delta_p}\right)^{0.5} \quad (3.51)$$

$$\phi = \frac{\tanh\left[\frac{m(W-D_o)}{2}\right]}{\left[\frac{m(W-D_o)}{2}\right]} \quad (3.52)$$

If the tubes are fabricated integral with the absorber plate, the adhesive resistance is neglected.

$$F = \frac{1}{WU_l\left[\frac{1}{U_l[(W-D_o)\phi+D_o]} + \frac{1}{\pi D_i h_f}\right]} \quad (3.53)$$

$$Q_u = F_R A_p\left[S - U_l\left(T_{fi} - T_a\right)\right] \quad (3.54)$$

$$F_R = \frac{\dot{m}C_p}{U_l A_p}\left[1 - \exp\left\{-\frac{FU_l A_p}{\dot{m}C_p}\right\}\right] \quad (3.55)$$

$$Q_u = \dot{m}C_p(T_{fo} - T_{fi}) \quad (3.56)$$

3.3.2 Input data

The various parameters for flat plate collector are mentioned below that have been used in MATLAB for the evaluation and analysis of gas filled solar flat plate collectors. The flat plate collector is made up of copper plate and copper tube fixed on the underside and one glass cover is taken [7].

- Length of collector = 2.08 m
- Width of collector = 1.07 m
- Length of absorber plate = 2 m
- Width of absorber plate = 0.98 m
- Plate to cover spacing (L) = 0.025 m
- Thermal conductivity of plate (K_P) = 350 W/m-K
- Plate thickness (δ_p) = 0.00015 m
- Absorptivity of plate for solar radiation (α) = 0.94
- Emissivity of plate for re-radiation (ε_p) = 0.14
- Outer diameter of tube (D_o) = 0.0137 m
- Inner diameter of tube (D_i) = 0.0125 m
- Tube centre to centre distance (W) = 0.113 m
- Glass cover emissivity/absorptivity = 0.88
- Glass cover thickness (d_c) = 0.004 m
- Extinction coefficient of glass(k_g) = 19 m^{-1}
- Refractive index of glass relative to air (μ) = 1.526
- Location of collector = Delhi (28.70° N, 77.10° E)
- Collector Tilt = Latitude Angle ($\beta = \emptyset$)
- Surface azimuth angle = 0° (As the inclined surface of collector faces due south)
- Adhesive resistance = Negligible
- Fluid to tube heat transfer coefficient (h_f) = 205 W/m^2-K
- Water mass flow rate ($\dot{m}$) = 70 kg/h or 0.019 kg/s
- Thickness of the back insulation (δ_b) = 0.05 m
- Thermal conductivity of the back insulation (k_i) = 0.04 (W/m-K)

- Reflectivity of surrounding surfaces (ρ) = 0.2
- Side loss coefficient is assumed to be 10% of the bottom loss coefficient

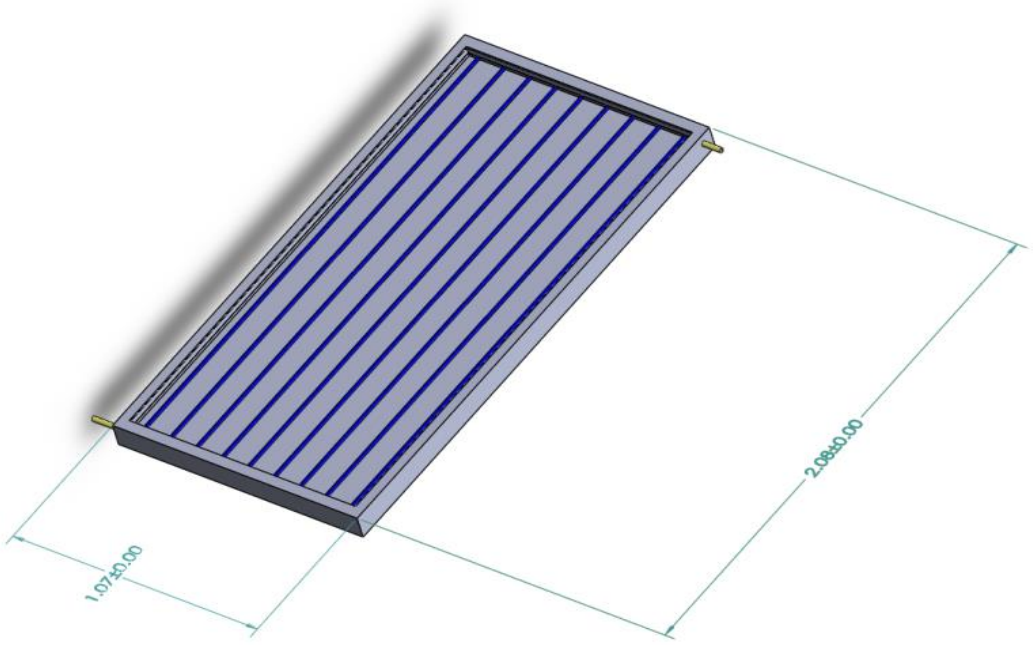

Fig.3.3 Outer dimensions of the flat plate collector

3.3.3 Procedure

The performance of various gas filled solar flat plate collectors have been compared with air filled solar flat plate collector in terms of instantaneous collector efficiency, heat transfer and overall loss coefficients on hourly basis from 08:00 to 17:00hrs Indian Standard Time (IST) and further the performance characteristic curve and equations of all eight solar flat plate collectors including air and other seven gases have been developed under clear sky conditions.

All the calculations involved in this analysis have been done in MATLAB 2018.The properties of various gases like thermal conductivity (k), coefficient of volume expansion (beta), Prandtl number (Pr) and kinematic viscosity (ν) is taken from EES (Engineering Equation Solver) S.A. Klein Professional V9.224-3D software at different temperatures. Pressure inside the spacing between the absorber plate and glass cover is

assumed to be 1 bar. The inlet temperature of water (T_{fi}) is taken as T_a+2°C for every calculation. Hourly radiation data of beam and diffuse radiation for all four months and ambient temperature at different time provided by IMD Pune mentioned in Appendix 1 is used to evaluate the performance of collectors from morning 8am to 5 pm evening (08:00 to 17:00 hrs.).Average wind speed is found as 2.83,3.48,2.63 and 2.28 m/s for January, June, August and October respectively [21]. The variation of the wind speed is shown in Appendix 2.

This evaluation is done for the clear sky conditions on 15thJanuary, 17thJune, 16th August and 20thOctober, the Hazy conditions on 17thJanuary, 16thJune, 18thAugust and 18thOctober, Hazy and cloudy conditions on 16thJanuary, 18thJune, 19thAugust and 17thOctober and the cloudy conditions on 18thJanuary, 20thJune, 20thAugust and 15thOctober.

The MATLAB program involves z value which has been used to select different gases while executing the program. The value of z has been assigned as 0,1,2,3,4,5,6 and 7 for air, carbon dioxide, methane, nitrous oxide, R410a, sulphur hexafluoride, R22 and R134a respectively. The properties are imported in MATLAB from EES for all the gases and those properties are coded with corresponding z value of that gas. These properties are imported at various temperatures with step size of 0.1 K. The codes involved in the MATLAB have been described in the form of flowchart in Fig.3.4.

3.3.4 Flowchart of MATLAB codes

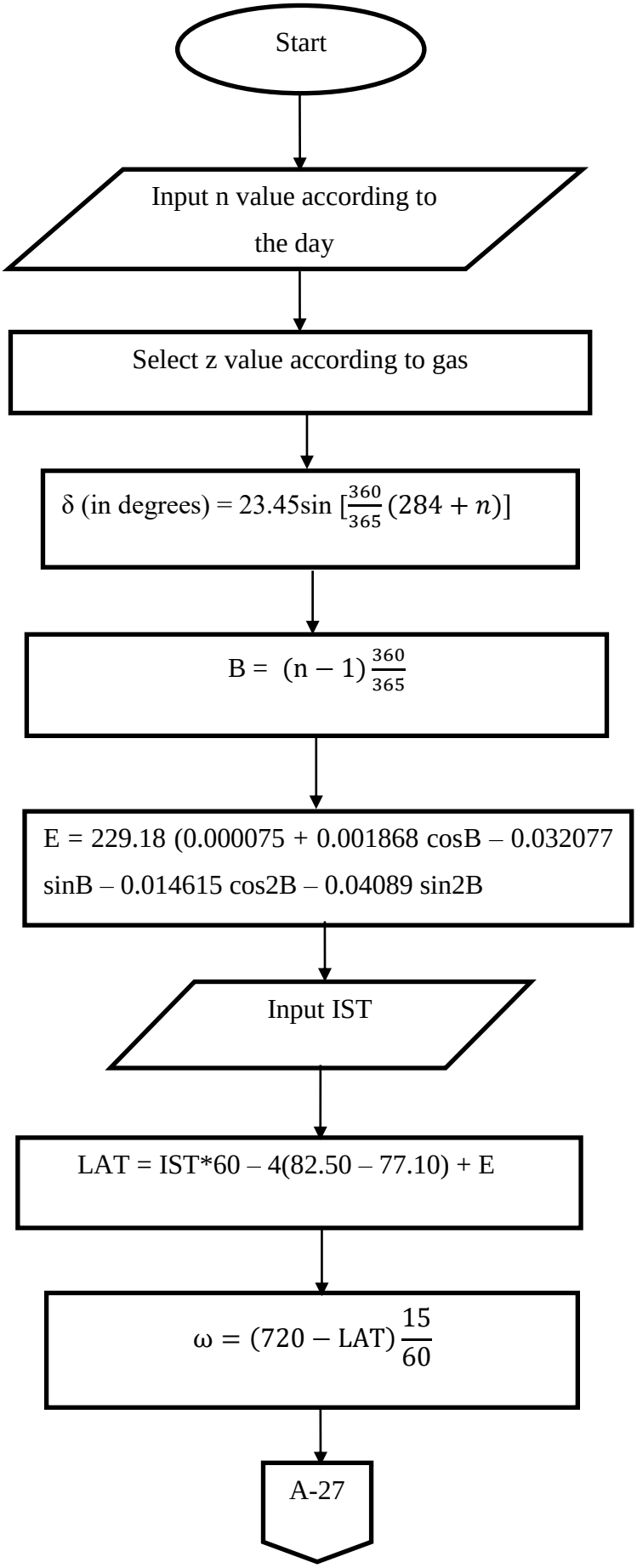

Contd.

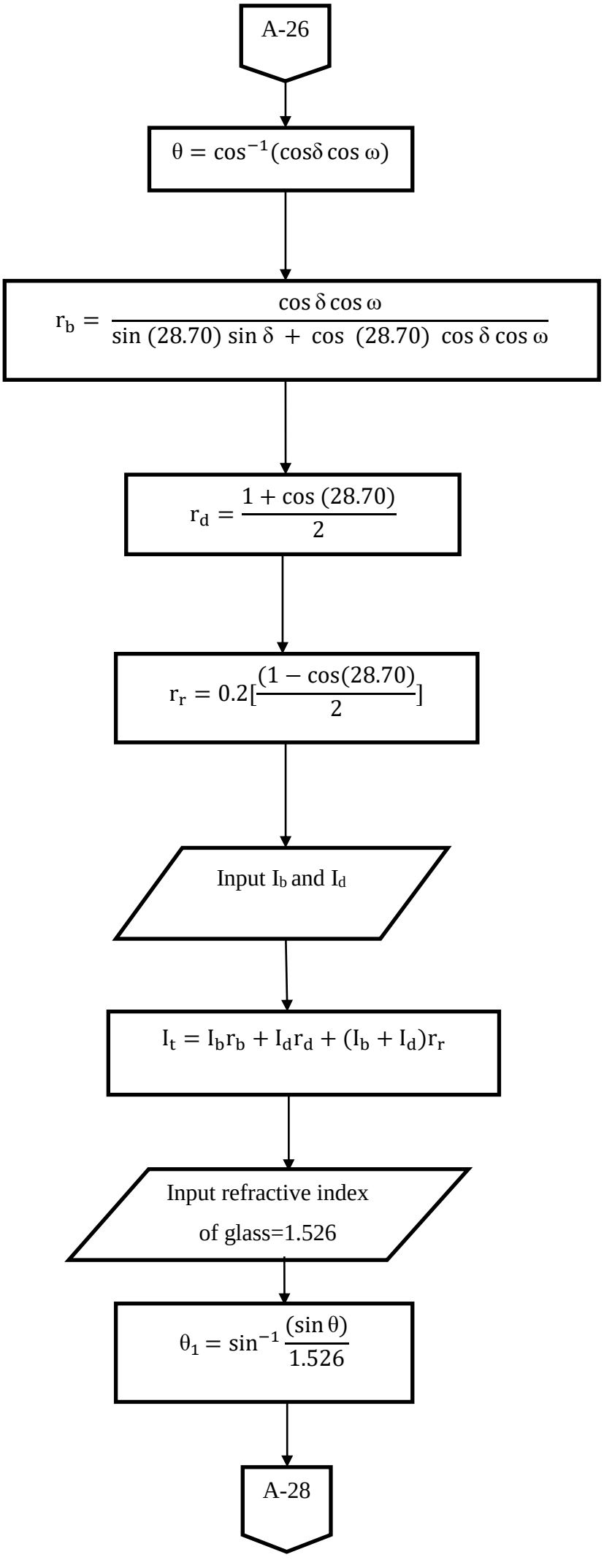
A-26
$\theta = \cos^{-1}(\cos\delta \cos \omega)$
$r_b = \frac{\cos \delta \cos \omega}{\sin (28.70) \sin \delta + \cos (28.70) \cos \delta \cos \omega}$
$r_d = \frac{1 + \cos (28.70)}{2}$
$r_r = 0.2[\frac{(1 - \cos(28.70)}{2}]$
Input I_b and I_d
$I_t = I_b r_b + I_d r_d + (I_b + I_d) r_r$
Input refractive index of glass=1.526
$\theta_1 = \sin^{-1} \frac{(\sin \theta)}{1.526}$
A-28

Contd.

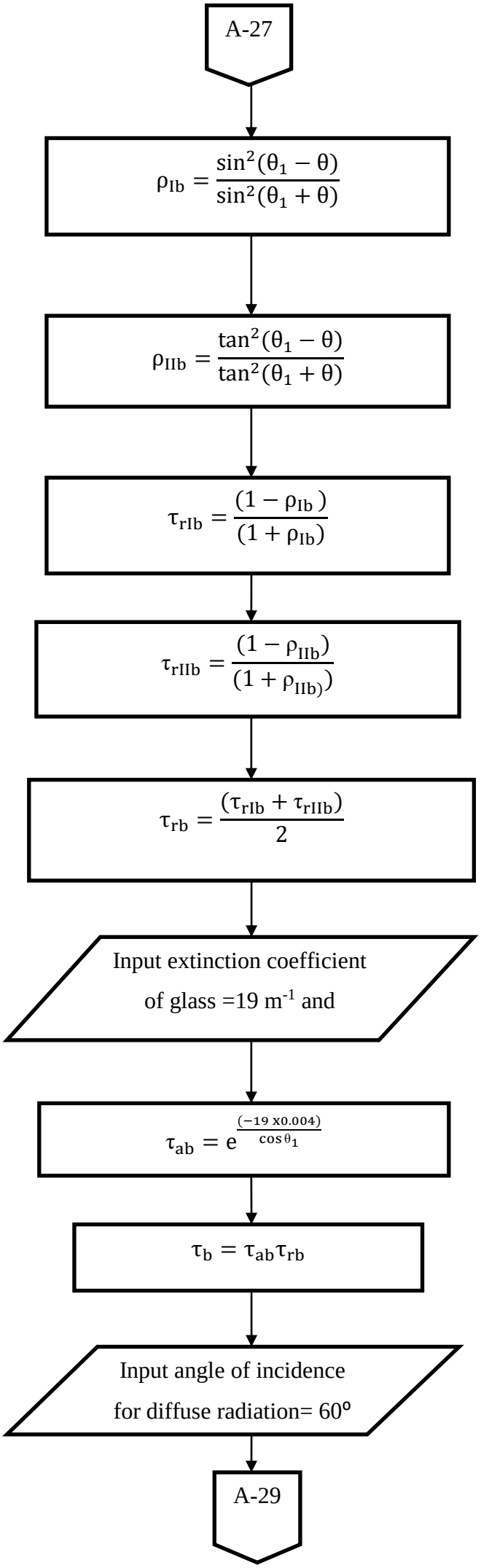
A-27
$\rho_{Ib} = \frac{\sin^2(\theta_1 - \theta)}{\sin^2(\theta_1 + \theta)}$
$\rho_{IIb} = \frac{\tan^2(\theta_1 - \theta)}{\tan^2(\theta_1 + \theta)}$
$\tau_{rIb} = \frac{(1 - \rho_{Ib})}{(1 + \rho_{Ib})}$
$\tau_{rIIb} = \frac{(1 - \rho_{IIb})}{(1 + \rho_{IIb})}$
$\tau_{rb} = \frac{(\tau_{rIb} + \tau_{rIIb})}{2}$
Input extinction coefficient of glass =19 m-1 and
$\tau_{ab} = e^{\frac{(-19 \text{ x} 0.004)}{\cos\theta_1}}$
$\tau_b = \tau_{ab}\tau_{rb}$
Input angle of incidence for diffuse radiation= 60°
A-29

Contd.

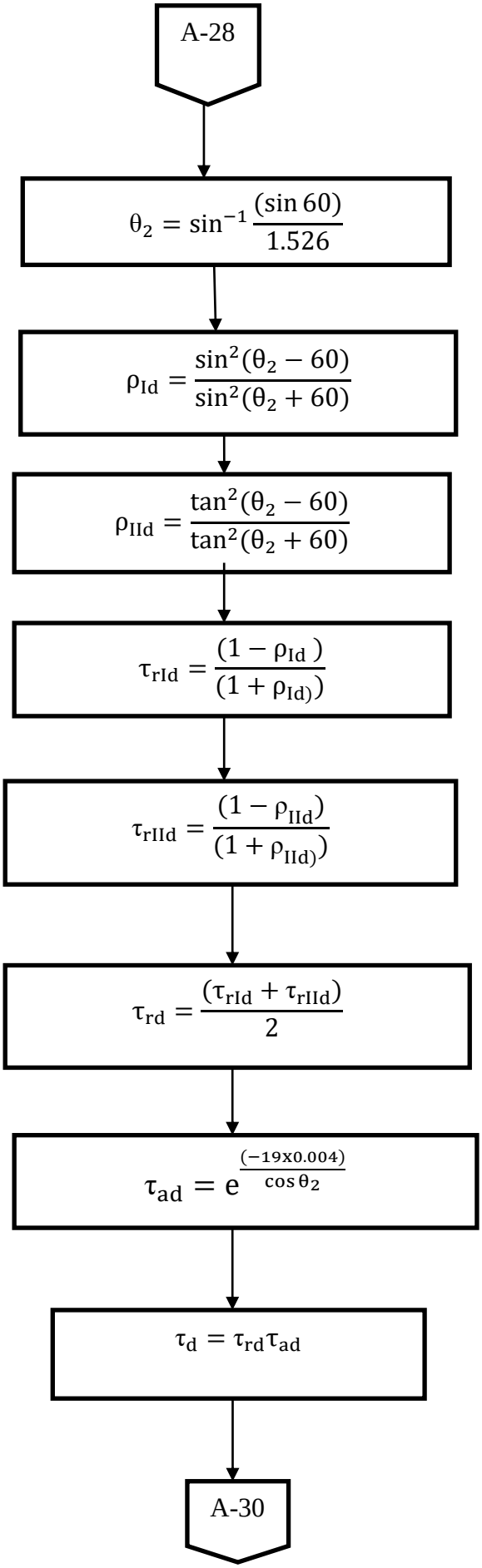
A-28
$\theta_2 = \sin^{-1}\frac{(\sin 60)}{1.526}$
$\rho_{Id} = \frac{\sin^2(\theta_2 - 60)}{\sin^2(\theta_2 + 60)}$
$\rho_{IId} = \frac{\tan^2(\theta_2 - 60)}{\tan^2(\theta_2 + 60)}$
$\tau_{rId} = \frac{(1 - \rho_{Id})}{(1 + \rho_{Id})}$
$\tau_{rIId} = \frac{(1 - \rho_{IId})}{(1 + \rho_{IId})}$
$\tau_{rd} = \frac{(\tau_{rId} + \tau_{rIId})}{2}$
$\tau_{ad} = e^{\frac{(-19x0.004)}{\cos\theta_2}}$
$\tau_d = \tau_{rd}\tau_{ad}$
A-30

Contd.

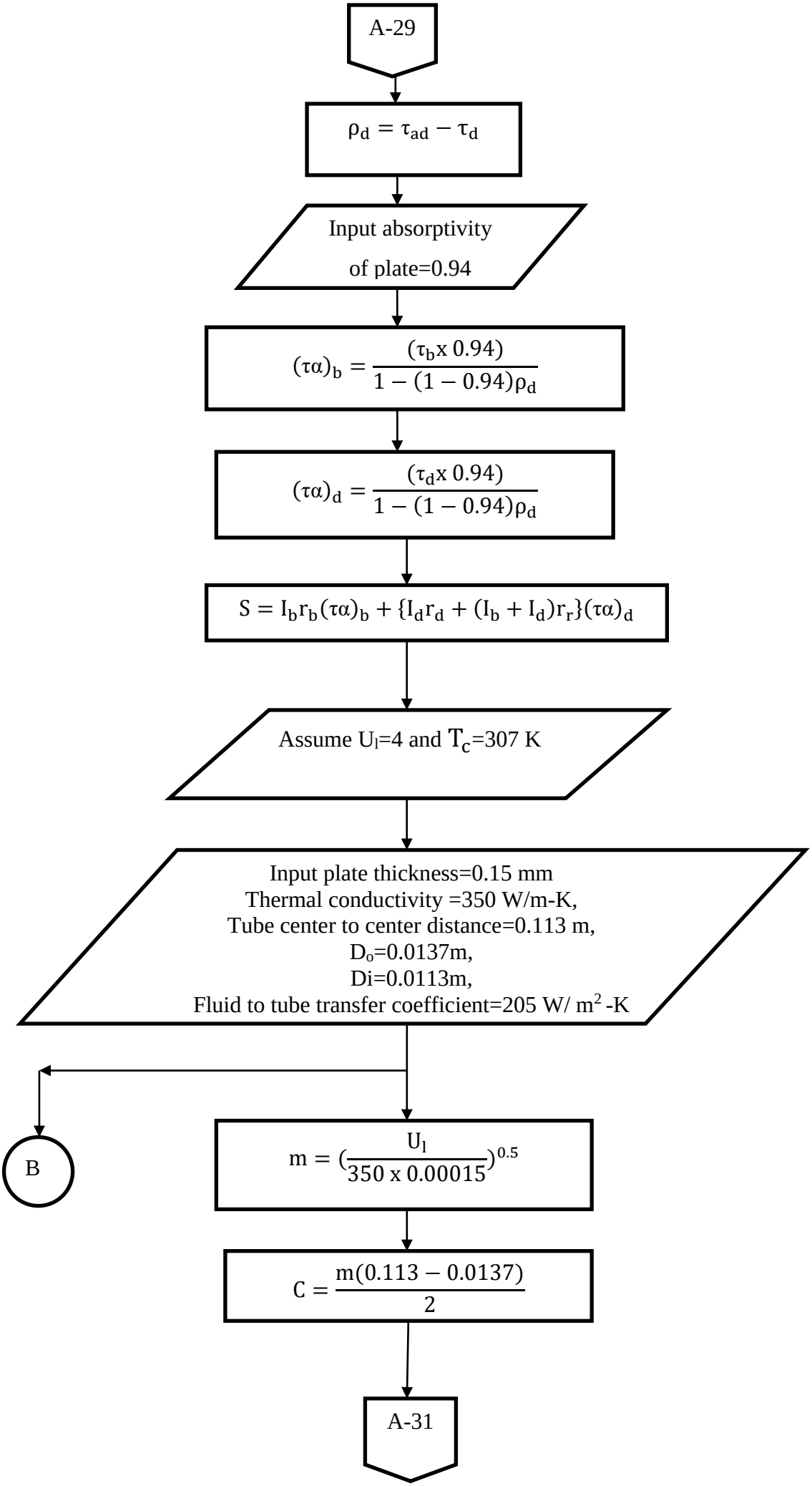
A-29
$\rho_d = \tau_{ad} - \tau_d$
Input absorptivity of plate=0.94
$(\tau\alpha)_b = \frac{(\tau_b x\ 0.94)}{1-(1-0.94)\rho_d}$
$(\tau\alpha)_d = \frac{(\tau_d x\ 0.94)}{1-(1-0.94)\rho_d}$
$S = I_b r_b (\tau\alpha)_b + \{I_d r_d + (I_b + I_d) r_r\}(\tau\alpha)_d$
Assume U_l=4 and T_c=307 K
Input plate thickness=0.15 mm
Thermal conductivity =350 W/m-K,
Tube center to center distance=0.113 m,
D_o=0.0137m,
Di=0.0113m,
Fluid to tube transfer coefficient=205 W/ m^2 -K
B
$m = (\frac{U_l}{350 \text{ x } 0.00015})^{0.5}$
$C = \frac{m(0.113 - 0.0137)}{2}$
A-31

Contd.

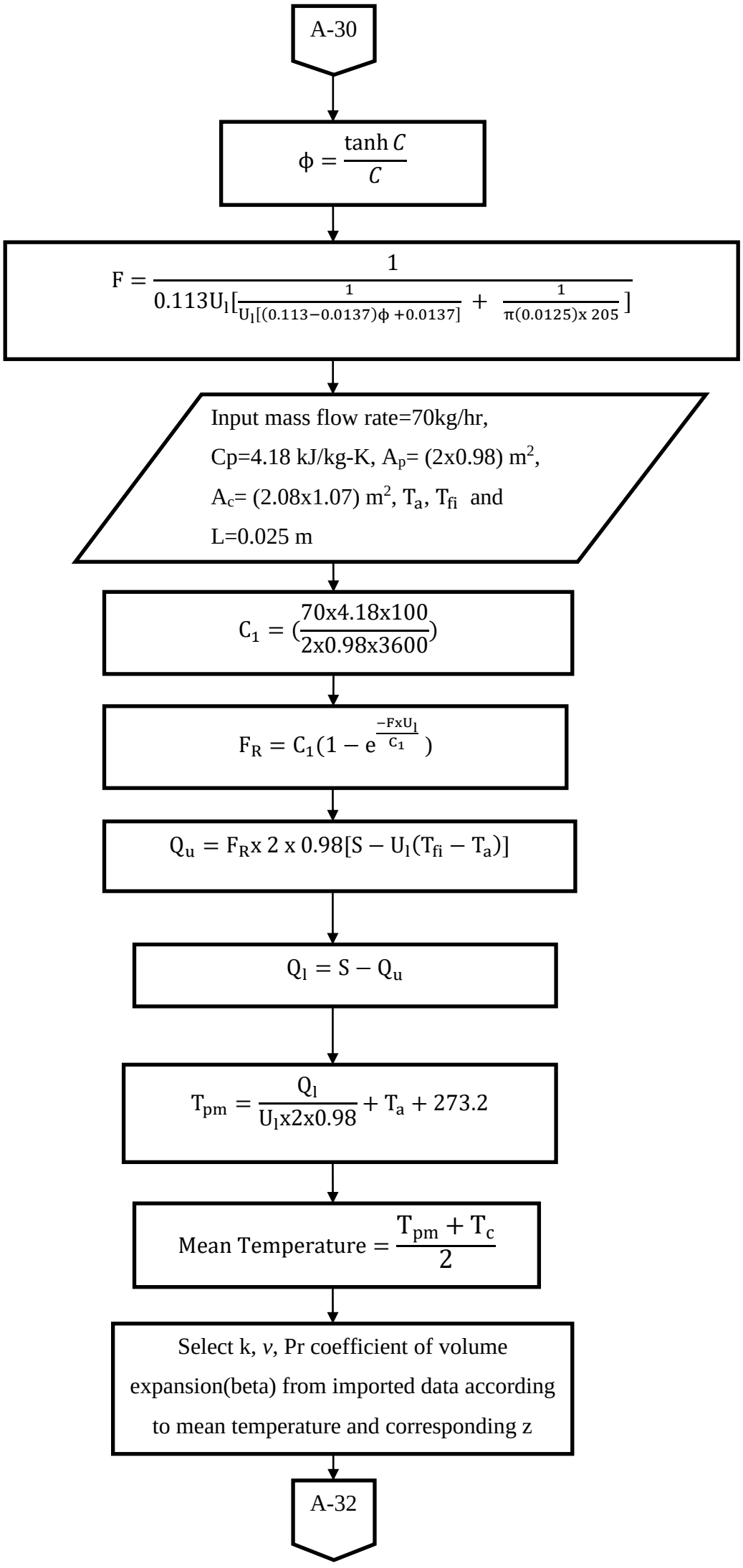
A-30
$\phi = \frac{\tanh C}{C}$
$F = \frac{1}{0.113U_l[\frac{1}{U_l[(0.113-0.0137)\phi + 0.0137]} + \frac{1}{\pi(0.0125)x\ 205}]}$
Input mass flow rate=70kg/hr,
Cp=4.18 kJ/kg-K, A_p= (2x0.98) m^2,
A_c= (2.08x1.07) m^2, T_a, T_{fi} and
L=0.025 m
$C_1 = (\frac{70x4.18x100}{2x0.98x3600})$
$F_R = C_1(1 - e^{\frac{-FxU_l}{C_1}})$
$Q_u = F_R x\ 2\ x\ 0.98[S - U_l(T_{fi} - T_a)]$
$Q_l = S - Q_u$
$T_{pm} = \frac{Q_l}{U_l x 2x0.98} + T_a + 273.2$
Mean Temperature $= \frac{T_{pm} + T_c}{2}$
Select k, *v*, Pr coefficient of volume expansion(beta) from imported data according to mean temperature and corresponding z
A-32

Contd.

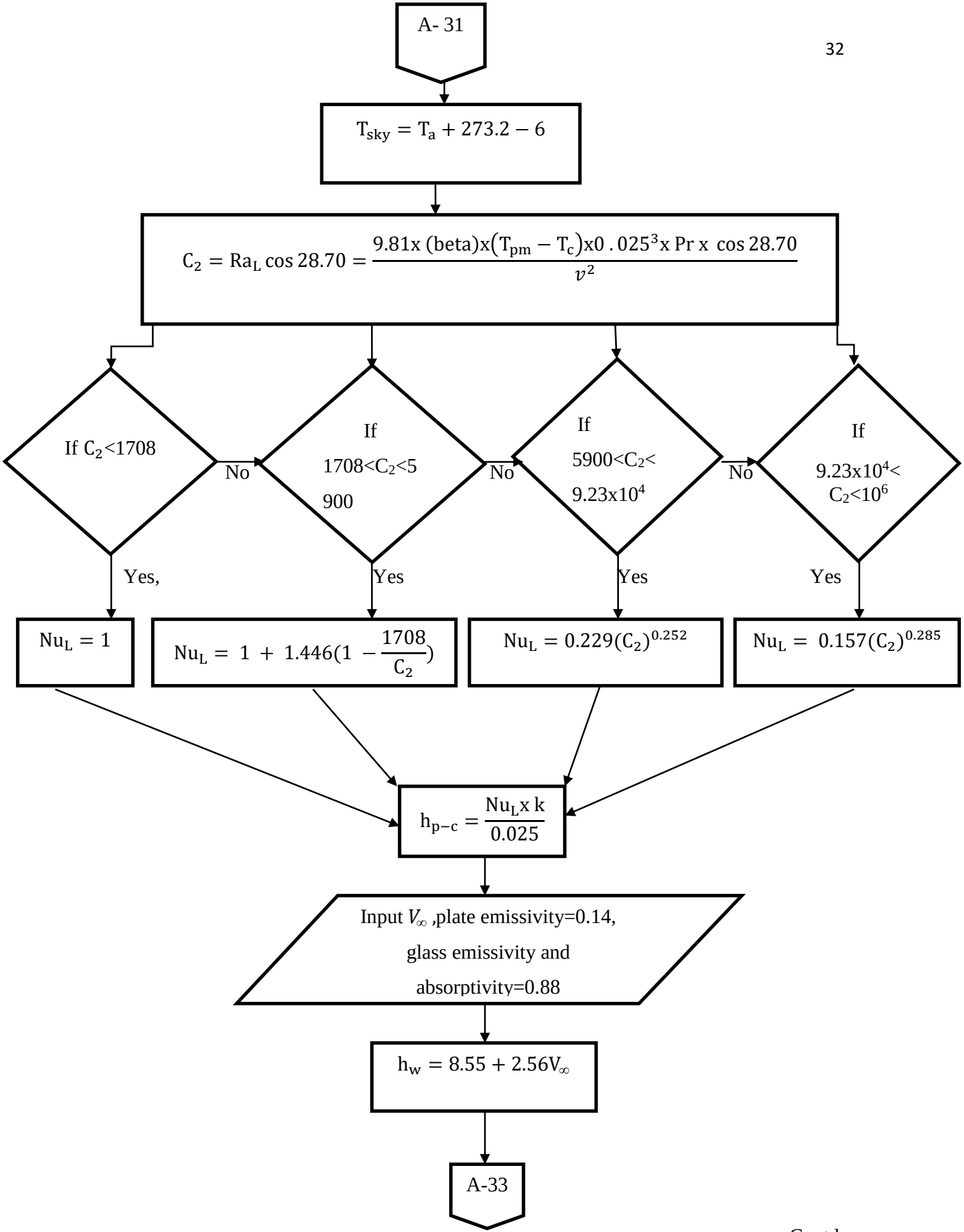
A- 31
$T_{sky} = T_a + 273.2 - 6$
$C_2 = Ra_L \cos 28.70 = \frac{9.81x\ (beta)x(T_{pm} - T_c)x0\ .\ 025^3x\ Pr\ x\ \cos 28.70}{v^2}$
If C_2<1708
No
If 1708<C_2<5900
No
If 5900<C_2< $9.23x10^4$
No
If $9.23x10^4$< C_2<10^6
Yes,
Yes
Yes
Yes
$Nu_L = 1$
$Nu_L = 1 + 1.446(1 - \frac{1708}{C_2})$
$Nu_L = 0.229(C_2)^{0.252}$
$Nu_L = 0.157(C_2)^{0.285}$
$h_{p-c} = \frac{Nu_L x\ k}{0.025}$
Input V_∞ ,plate emissivity=0.14, glass emissivity and absorptivity=0.88
$h_w = 8.55 + 2.56V_\infty$
A-33

Contd.

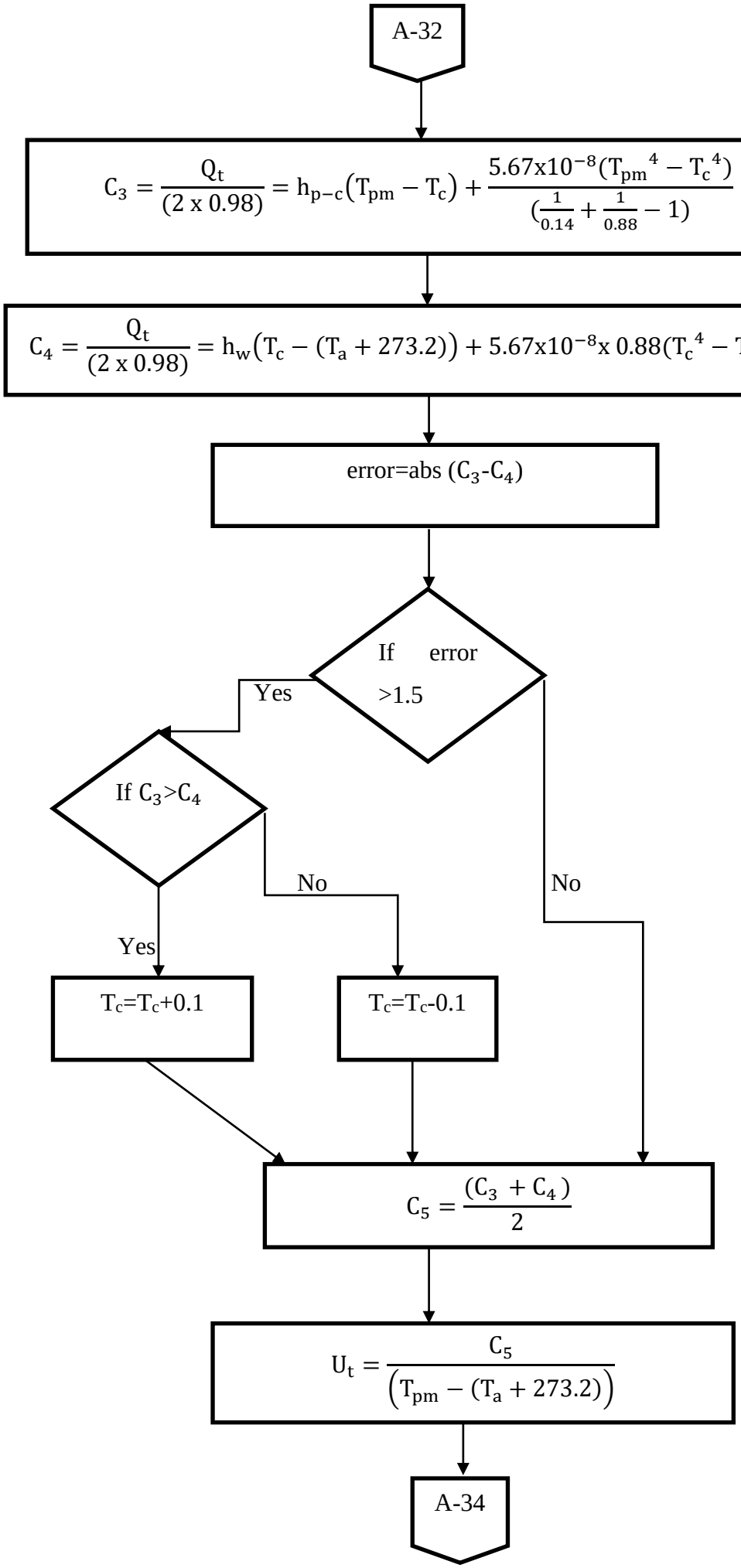
A-32
$C_3 = \frac{Q_t}{(2 \times 0.98)} = h_{p-c}(T_{pm} - T_c) + \frac{5.67x10^{-8}({T_{pm}}^4 - {T_c}^4)}{(\frac{1}{0.14} + \frac{1}{0.88} - 1)}$
$C_4 = \frac{Q_t}{(2 \times 0.98)} = h_w(T_c - (T_a + 273.2)) + 5.67x10^{-8} x\ 0.88({T_c}^4 - {T_{sky}}^4)$
error=abs (C_3-C_4)
If error >1.5
Yes
No
If C_3>C_4
Yes
No
T_c=T_c+0.1
T_c=T_c-0.1
$C_5 = \frac{(C_3 + C_4)}{2}$
$U_t = \frac{C_5}{(T_{pm} - (T_a + 273.2))}$
A-34

Contd.

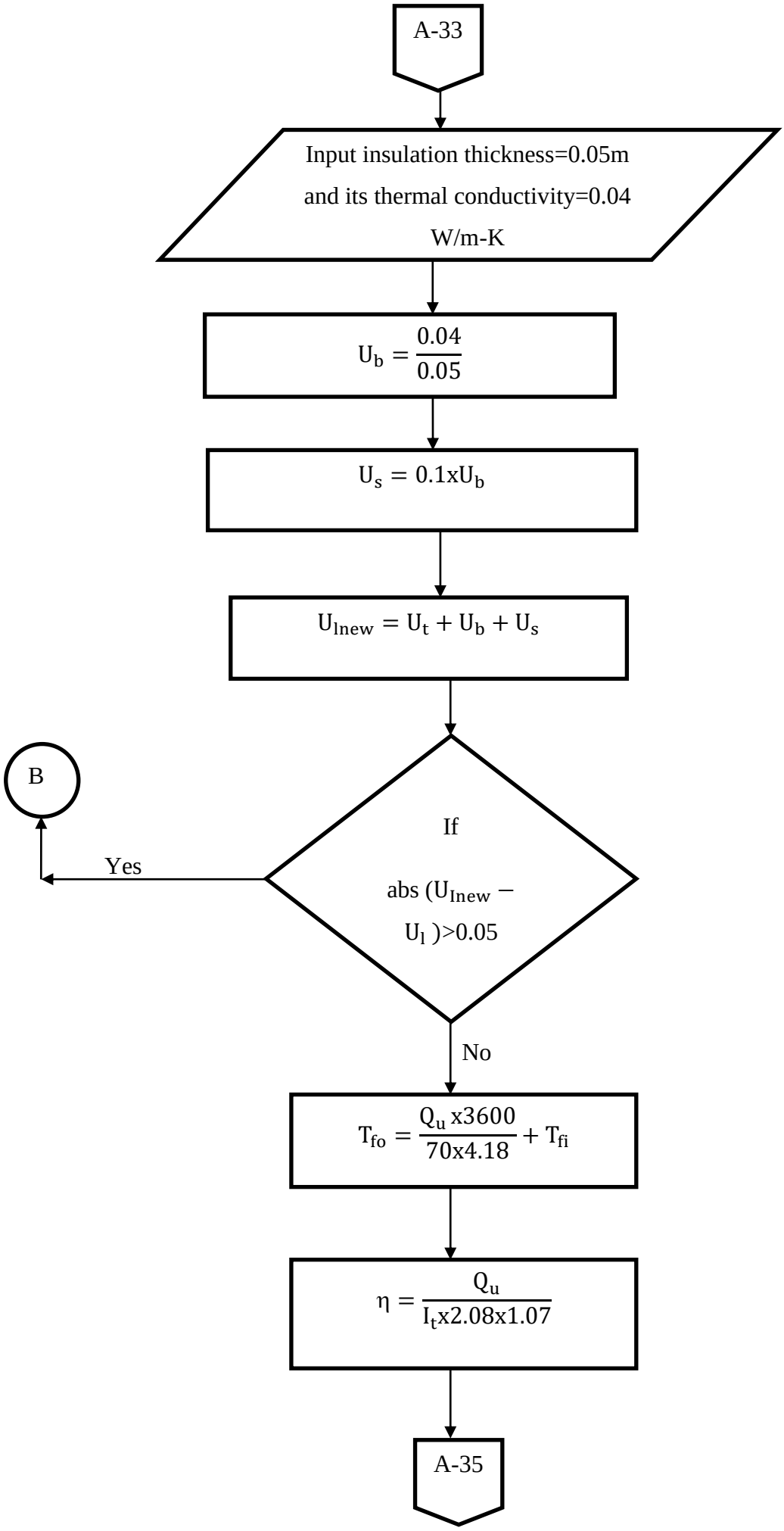
A-33
Input insulation thickness=0.05m and its thermal conductivity=0.04 W/m-K
$U_b = \frac{0.04}{0.05}$
$U_s = 0.1xU_b$
$U_{lnew} = U_t + U_b + U_s$
If abs ($U_{Inew} - U_l$)>0.05
Yes
B
No
$T_{fo} = \frac{Q_u x3600}{70x4.18} + T_{fi}$
$\eta = \frac{Q_u}{I_t x2.08x1.07}$
A-35

Contd.

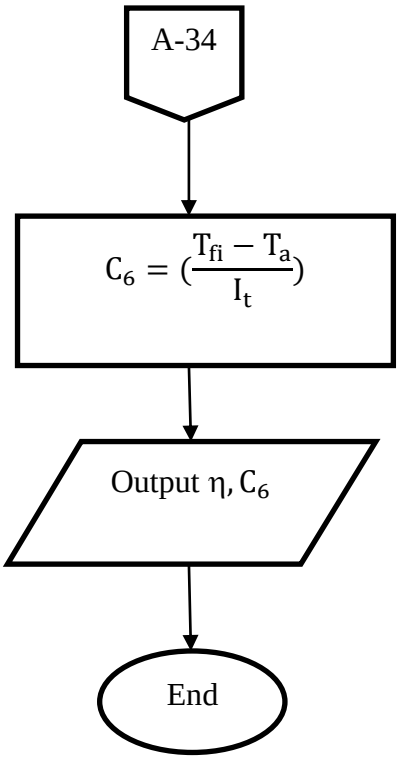

Fig.3.4 Flowchart of MATLAB codes

CHAPTER 4

RESULTS AND DISCUSSIONS

This chapter deals with discussions on results obtained from the performance analysis of gas filled solar flat plate collectors. The performance of all gas filled solar flat plate collector is compared with the air-filled flat collector in terms of instantaneous efficiency for four months under four different climatic conditions. Further, the overall heat loss coefficient and convective heat transfer coefficient between the absorber plate and glass cover of gas filled collectors is analyzed. Also, the performance characteristic curves and equations are developed under clear sky condition.

4.1 Efficiency of gas filled collectors

4.1.1 In the month of January

4.1.1.1 Clear sky condition

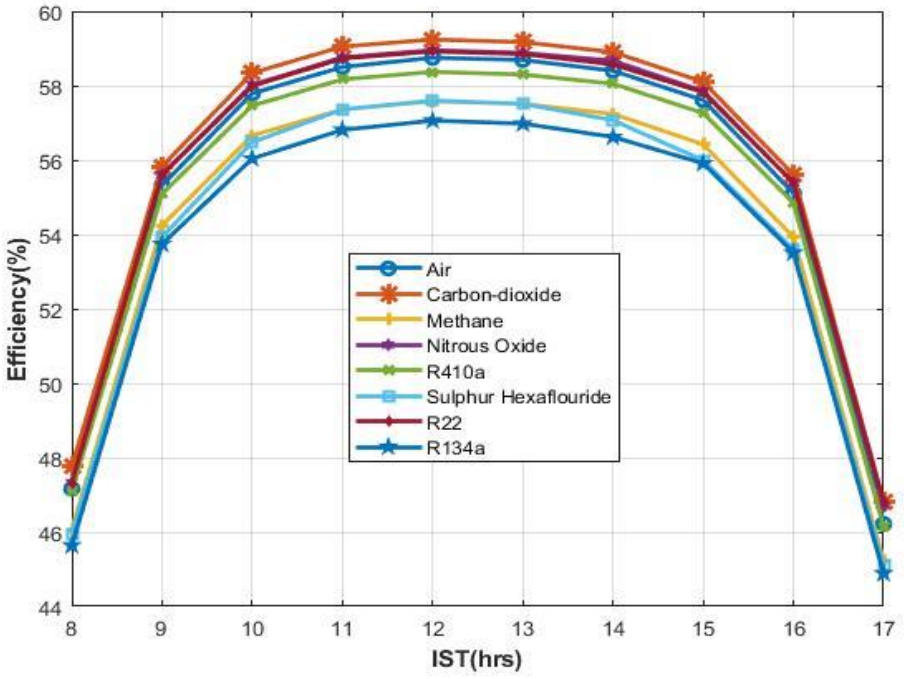

Fig.4.1 Efficiency under clear sky condition in January

Fig.4.1 shows the variation of instantaneous efficiency over a day under clear sky condition (15thJanuary, 2016). The carbon dioxide gas filled collector has 0.95% increase in average efficiency over the day (8:00 to 17:00hrs.) compared to air filled solar flat plate collector. There is slight increase in average efficiency for nitrous oxide and R22 filled solar collector i.e. 0.47 and 0.45% for nitrous oxide and R22 respectively. Other four gas filled collectors i.e. methane, R410a, sulphur hexafluoride (SF_6), R134a do not show increase in efficiency.

4.1.1.2 Hazy day

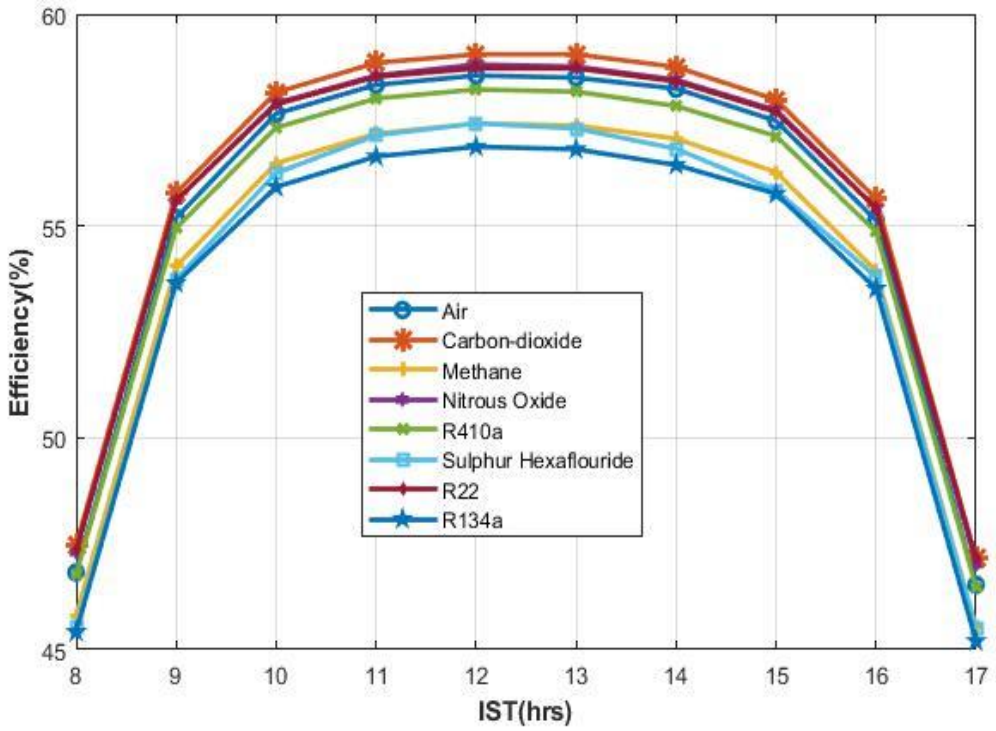

Fig.4.2 Efficiency under hazy condition in January.

Fig.4.2 shows the variation of instantaneous efficiency over a day under hazy condition (17thJanuary, 2016). It is seen that carbon dioxide gas filled collector has 1% increase in average efficiency over the day compared to air filled solar flat plate collector. Nitrous oxide filled collector shows 0.56% and R22 filled collector shows 0.55% increase in their average efficiency. Remaining gas filled collectors have lower efficiency than air filled collector.

4.1.1.3 Hazy and cloudy day

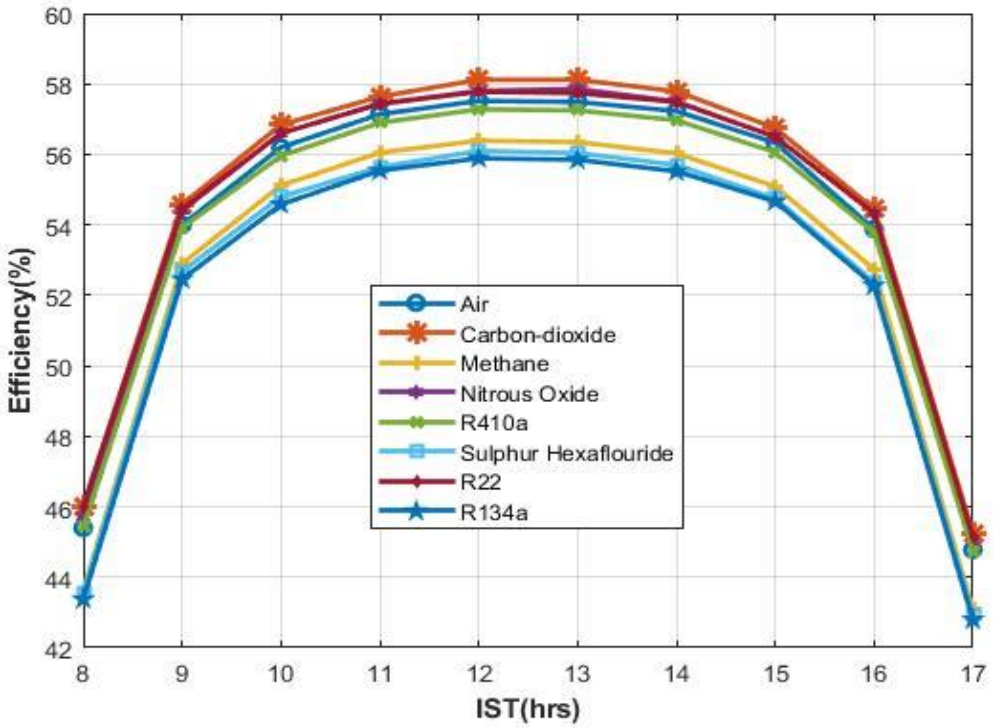

Fig.4.3 Efficiency under hazy and cloudy conditions in January

Fig.4.3 shows the variation of instantaneous efficiency over a day under hazy and cloudy condition (16th January, 2016). There is 1.03% increase in average efficiency for carbon dioxide filled solar collector and 0.60 and 0.65% increase in average efficiency for nitrous oxide and R22 gas filled collectors respectively. Remaining gas filled solar flat plate collectors have lower efficiency than air filled solar flat plate collector.

4.1.1.4 Cloudy condition

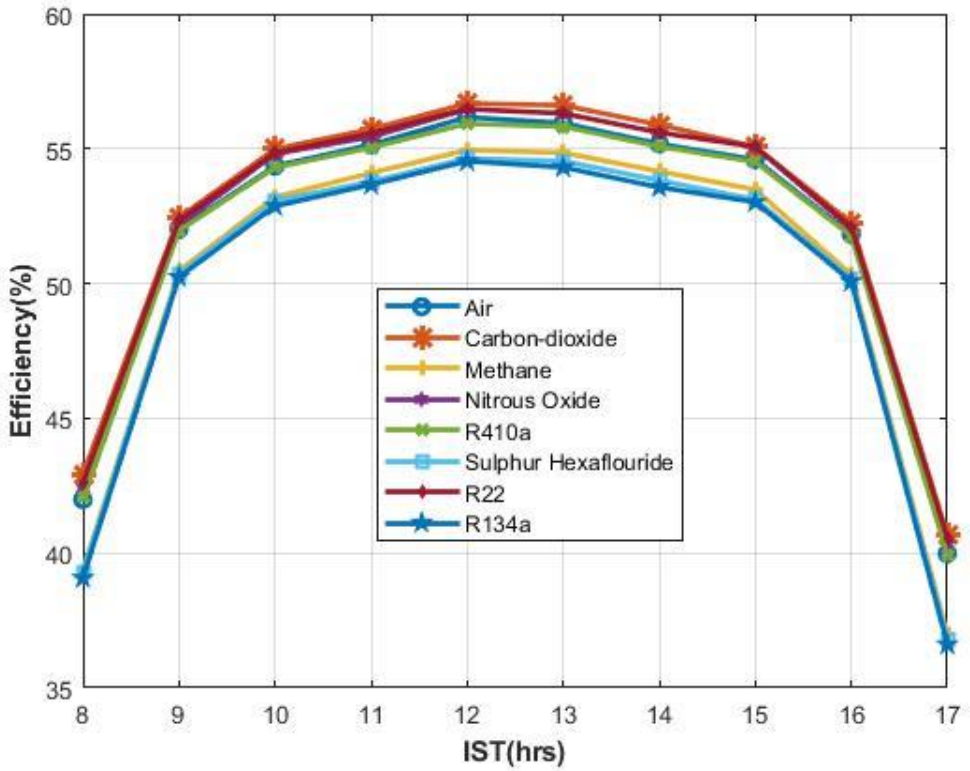

Fig.4.4 Efficiency under cloudy condition in January

Fig.4.4 shows the variation of instantaneous efficiency over a day under cloudy condition (18th January, 2016). It is seen that carbon dioxide filled collector has increase of 1.17% in average efficiency. Nitrous oxide filled collector shows 0.66% increase and R22 filled one shows 0.83% increase in their average efficiency. Other gas filled collectors have lower efficiency than air filed solar flat plate collector.

4.1.2 In the month of June

4.1.2.1 Clear sky condition

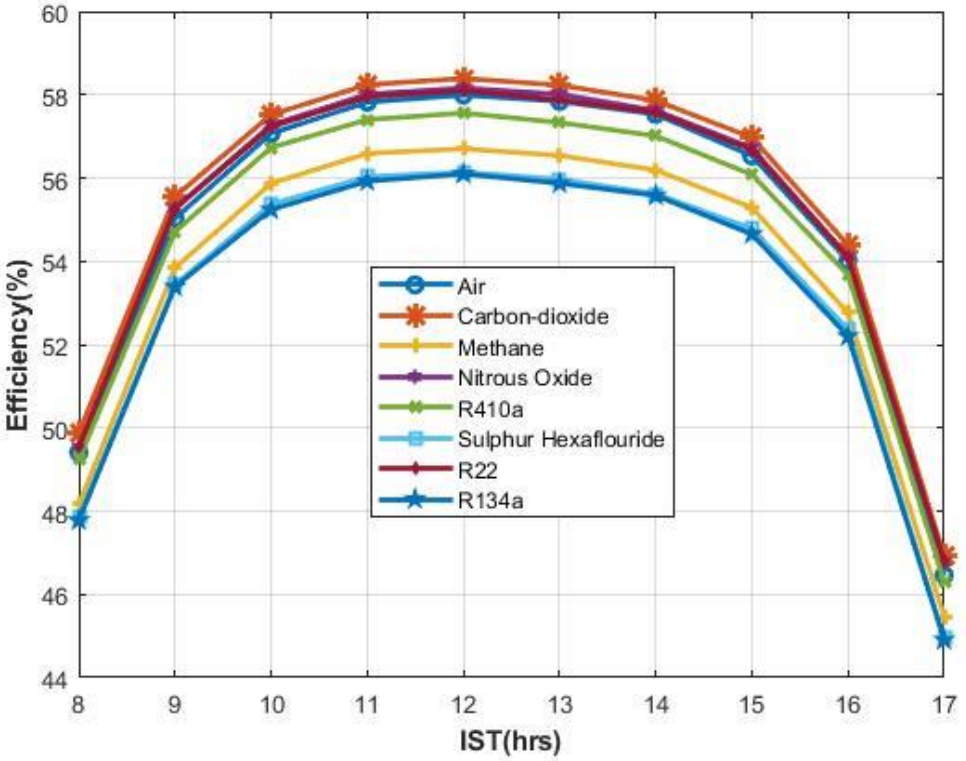

Fig.4.5 Efficiency under clear sky condition in June

Fig. 4.5 shows the variation of instantaneous efficiency over a day under clear sky condition (17th June, 2016). The carbon dioxide gas filled collector has 0.77% increase in average efficiency over the day (8:00 to 17:00hrs.) as compared to air filled solar flat plate collector. There is slight increase in average efficiency for nitrous oxide and R22 filled solar collectors i.e. 0.33% and 0.26% for nitrous oxide and R22 respectively. Other four gas filled solar flat plate collectors i.e. methane, R410a, sulphur hexafluoride (SF_6), R134a do not show increase in efficiency.

4.1.2.2 Hazy day

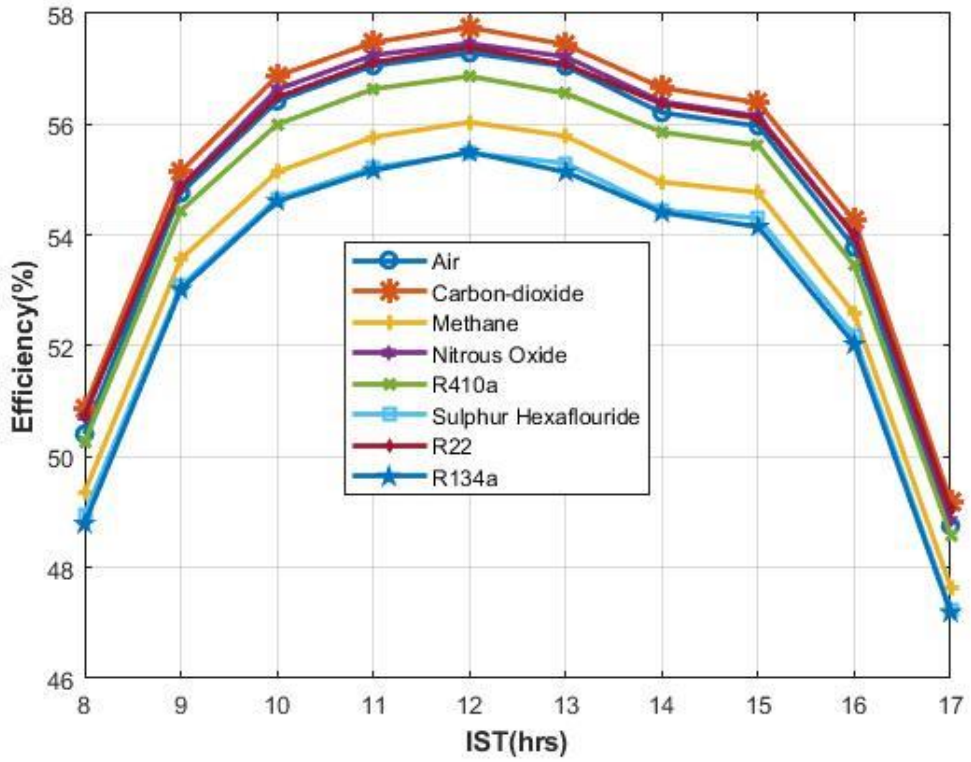

Fig.4.6 Efficiency under hazy condition in June

Fig.4.6 shows the variation of instantaneous efficiency over a day under hazy condition (16th June, 2016). The carbon dioxide gas filled collector has 0.80% increase in average efficiency over the day compared to air filled solar flat plate collectors. Nitrous oxide filled collector shows 0.34% and R22 filled collector shows 0.28% increase in their average efficiency. Remaining gas filled solar flat plate collectors have lower efficiency than air filled solar flat plate collector.

4.1.2.3 Hazy and cloudy condition

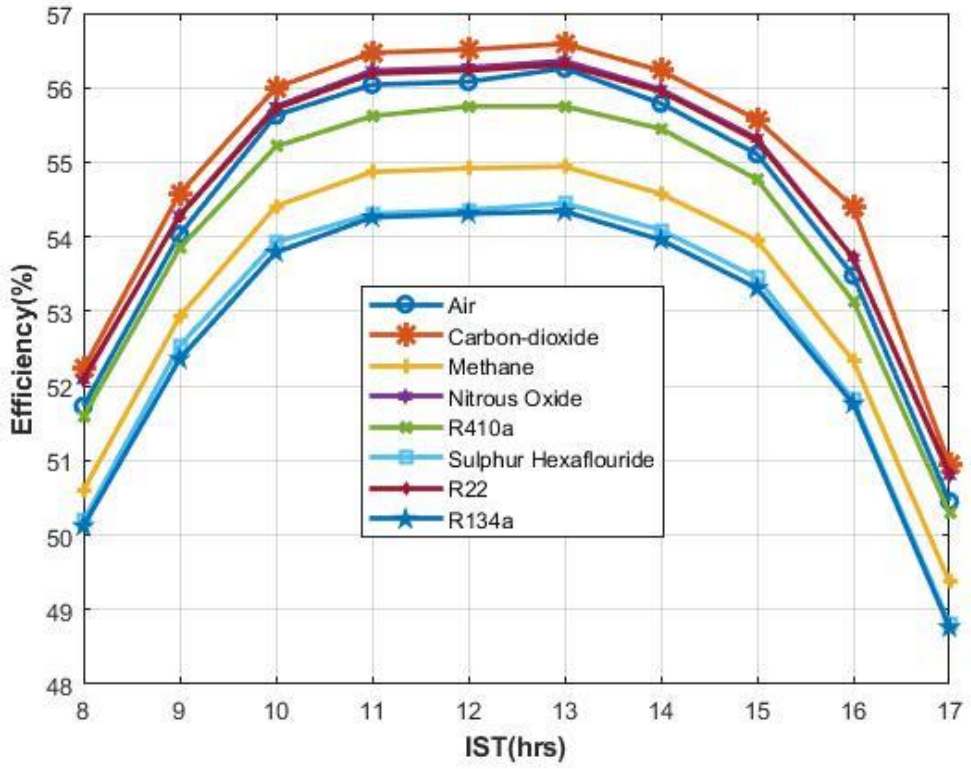

Fig.4.7 Efficiency under hazy and cloudy condition in June

Fig.4.7 shows the variation of instantaneous efficiency over a day under hazy and cloudy condition (18th June, 2016). There is 0.91% increase in average efficiency for carbon dioxide filled solar collector and 0.40 and 0.37% increase in average efficiency for nitrous oxide and R22 gas filled collectors respectively. Remaining gas filled solar flat plate collectors have lower efficiency than air filled solar flat plate collector.

4.1.2.4 Cloudy condition

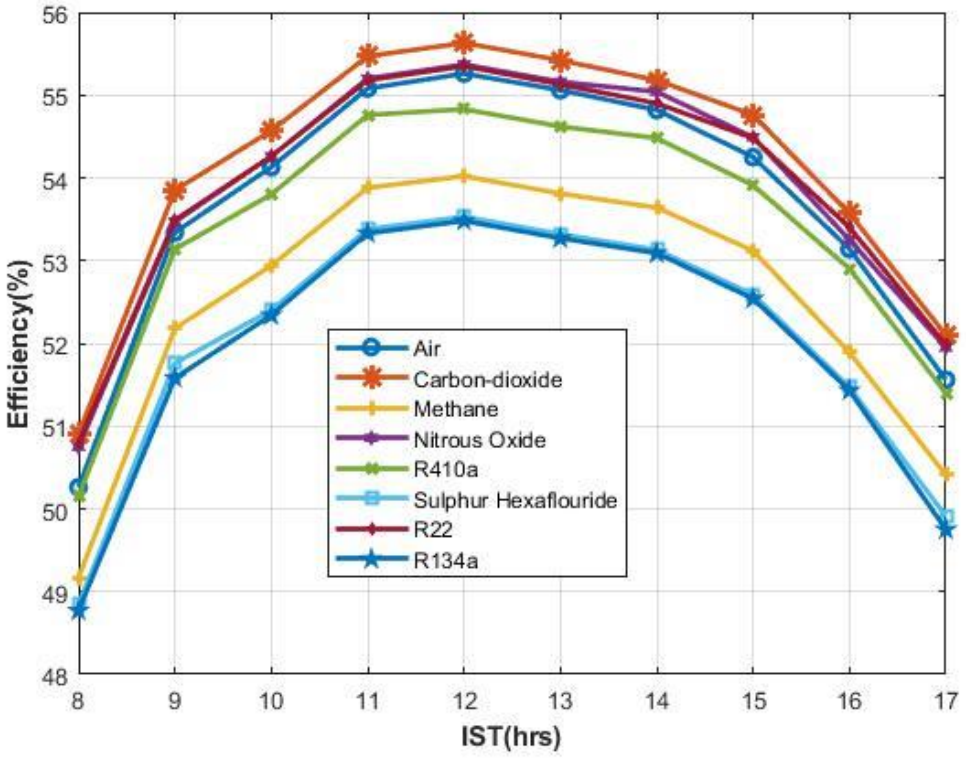

Fig.4.8 Efficiency under cloudy condition in June

Fig.4.8 shows the variation of instantaneous efficiency over a day under cloudy condition (20thJune, 2016). The carbon dioxide filled collector has increase of 0.85% in average efficiency compared to air filled solar flat plate collector. Nitrous oxide filled collector shows 0.38% increase and R22 filled one shows 0.39% increase in their average efficiency. Other gas filled solar collectors have lower efficiency than air filed solar flat plate collector.

4.1.3 In the month of August

4.1.3.1 Clear sky condition

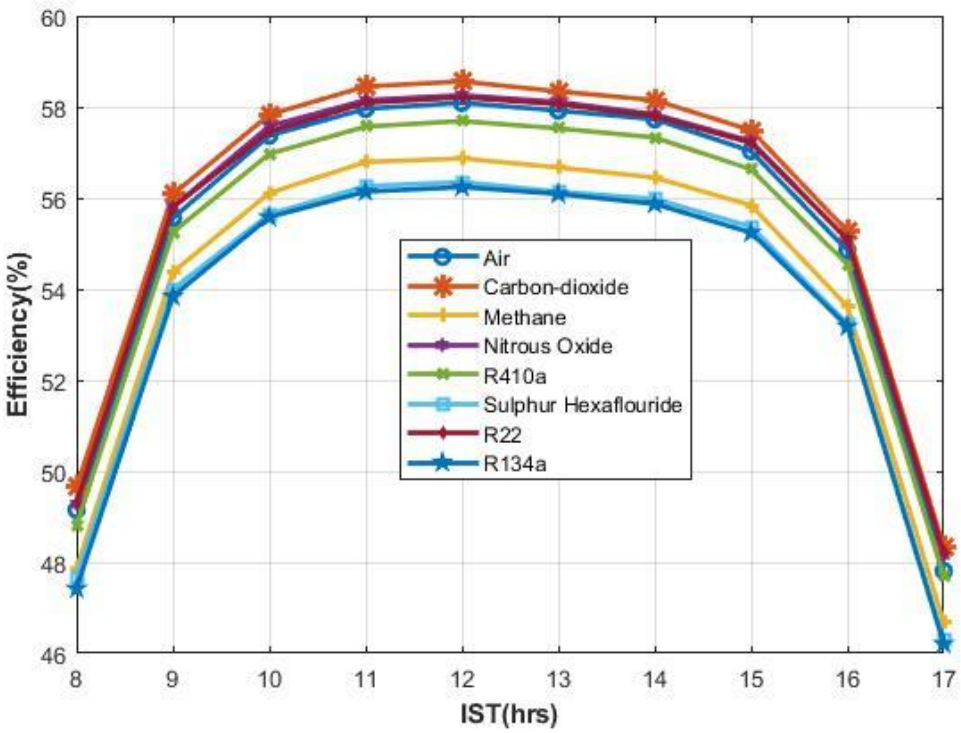

Fig.4.9 Efficiency under clear sky condition in August

Fig.4.9 shows the variation of instantaneous efficiency over a day under clear sky condition (16th August, 2016). It is observed that carbon dioxide gas filled collector has 0.85% increase in average efficiency over the day compared to air filled solar flat plate collector. There is some slight increase in average efficiency for nitrous oxide and R22 filled solar collectors i.e. 0.37 and 0.32% for nitrous oxide and R22 respectively. Other four gas filled collectors i.e. methane, R410a, sulphur hexafluoride (SF_6), R134a have lower efficiency than air filled collector.

4.1.3.2 Hazy day

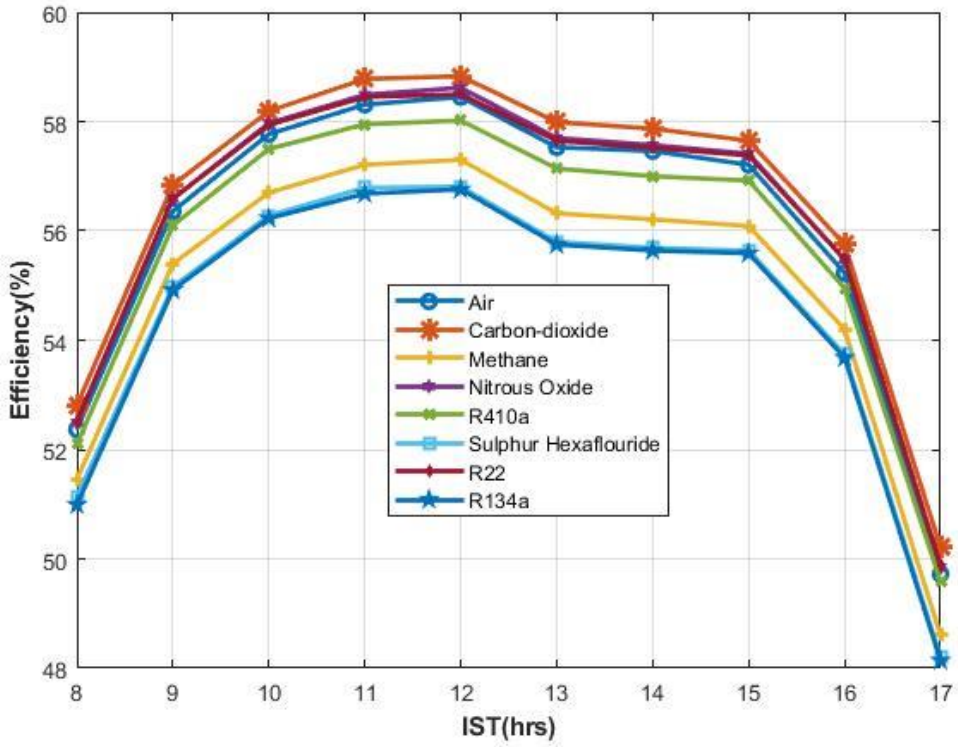

Fig.4.10 Efficiency under hazy condition in August

Fig.4.10 shows the variation of instantaneous efficiency over a day under hazy condition (18thAugust, 2016). The carbon dioxide gas filled collector has 0.80% increase in average efficiency over the day compared to air filled solar flat plate collectors. Nitrous oxide filed solar flat plate collector show 0.31% and R22 filed solar flat plate collector shows 0.27% increase in their average efficiency. Remaining gas filled solar flat plate collectors have lower efficiency than air filed solar flat plate collector.

4.1.3.3 Haze and cloudy condition

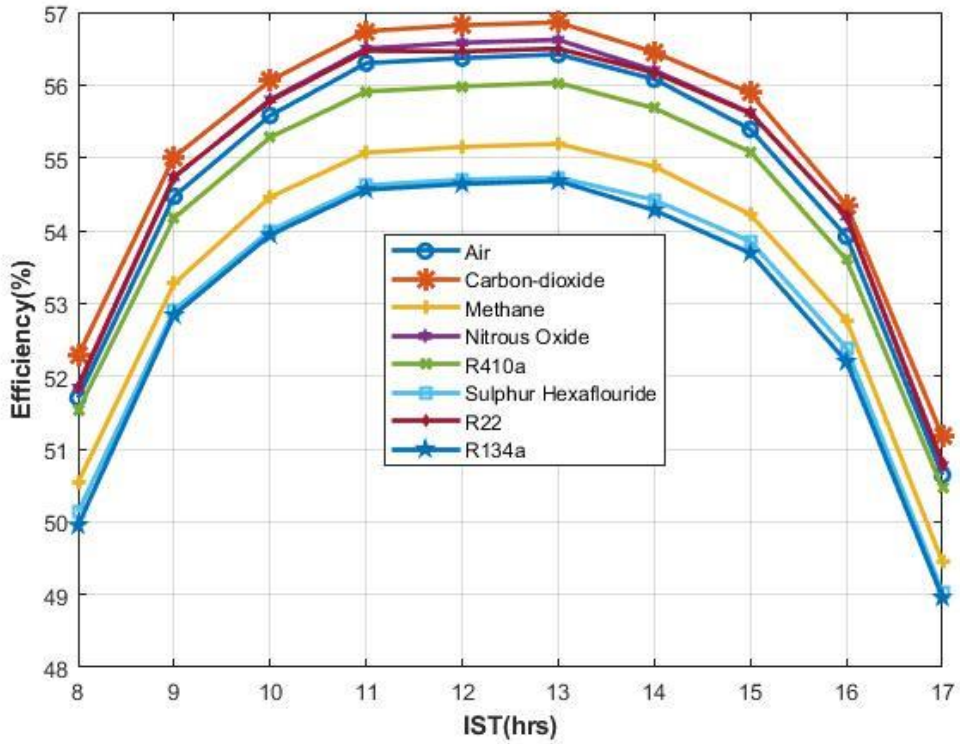

Fig.4.11 Efficiency under haze and cloudy condition in August

Fig.4.11 shows the variation of instantaneous efficiency over a day under haze and cloudy condition (19th August, 2016). There is 0.87% increase in average efficiency for carbon dioxide filled solar collector. There is 0.36 and 0.32% increase in average efficiency for nitrous oxide and R22 filled collectors respectively. Other gas filled collectors do not show increase in average efficiency compared to air solar flat plate collector.

4.1.3.4 Cloudy conditions

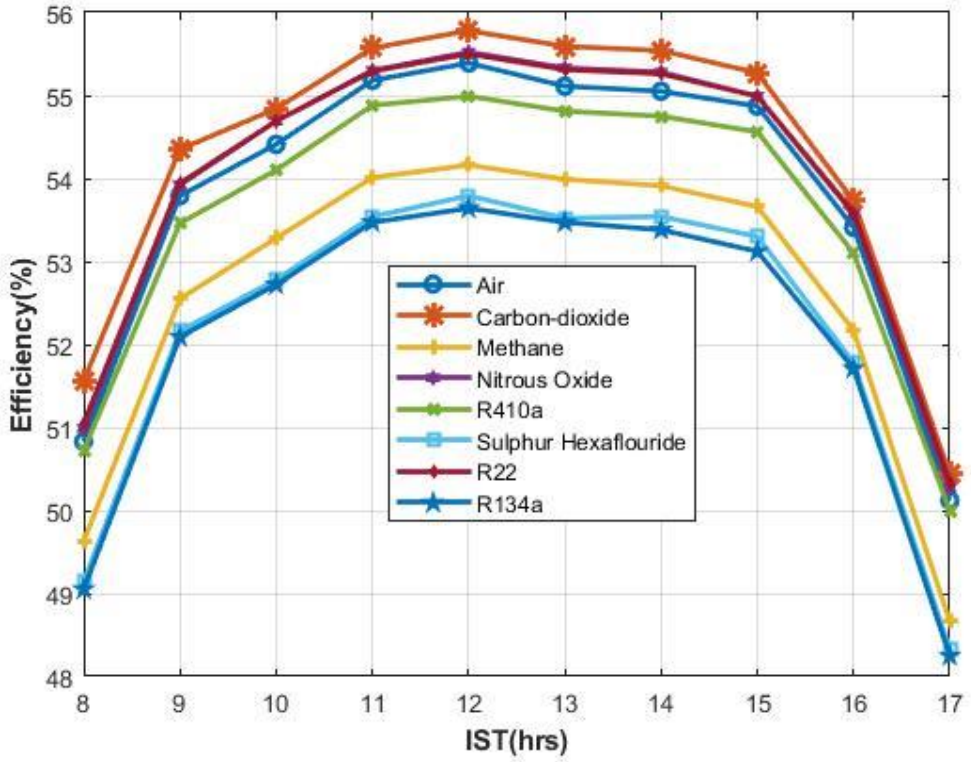

Fig.4.12 Efficiency under cloudy condition in August

Fig.4.12 shows the variation of instantaneous efficiency over a day under cloudy condition (20th August, 2016). The carbon dioxide filled collector has increase of 0.84% in average efficiency. Nitrous oxide filled collector shows 0.32% increase and R22 filled one show 0.33% increase in their efficiency compared to air filled solar flat plate collector. Other gas filled solar flat plate collectors have lower efficiency than air filled solar flat plate collector.

4.1.4 In the month of October

4.1.4.1 Clear sky condition

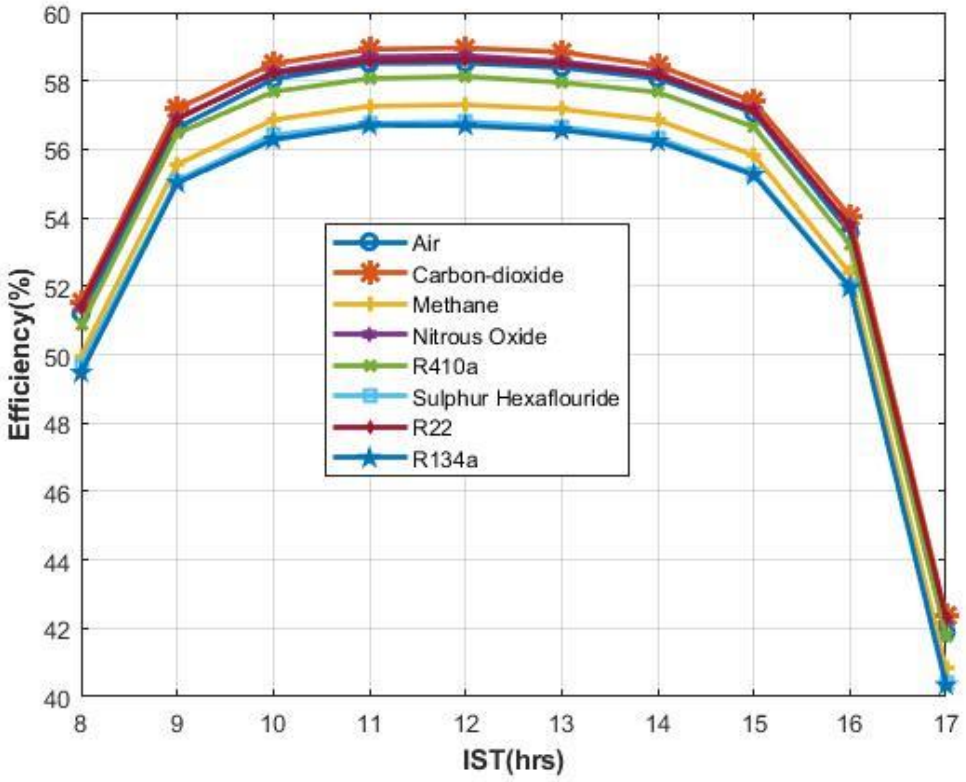

Fig.4.13 Efficiency under clear sky condition in October

Fig.4.13 shows the variation of instantaneous efficiency over a day under clear sky condition (20th October, 2016). The carbon dioxide gas filled collector has 0.79% increase in average efficiency over the day compared to air filled solar flat plate collectors. There is some slight increase in average efficiency for nitrous oxide and R22 filled solar collectors i.e. 0.38 and 0.31% for nitrous oxide and R22 respectively. Other four gas filled collectors i.e. methane, R410a, sulphur hexafluoride (SF_6), R134a do not show increase in efficiency.

4.1.4.2 Hazy condition

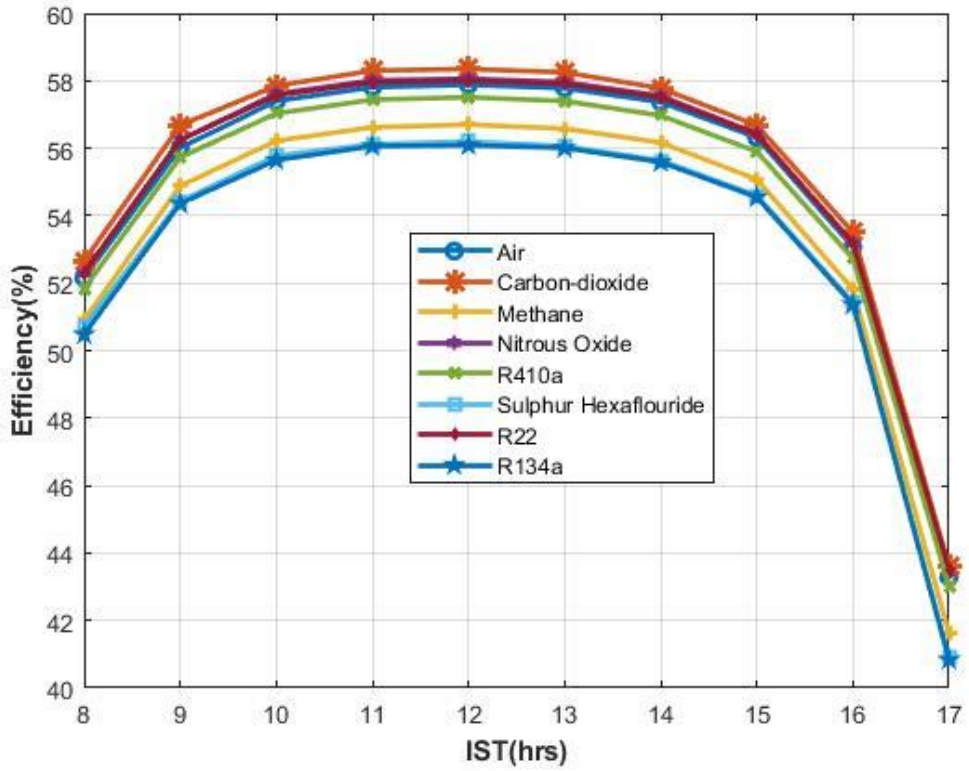

Fig.4.14 Efficiency under hazy condition in October

Fig.4.14 shows the variation of instantaneous efficiency over a day under hazy condition (18thOctober, 2016). The carbon dioxide gas filled collector has 0.83% increase in average efficiency over the day compared to air filled solar flat plate collectors. Nitrous oxide filled collector shows just 0.30% and R22 filled collector shows just 0.28% increase in their average efficiency. Other gas filled collectors do not show increase in average efficiency compared to air solar flat plate collector.

4.1.4.3 17 October-Hazy and cloudy condition

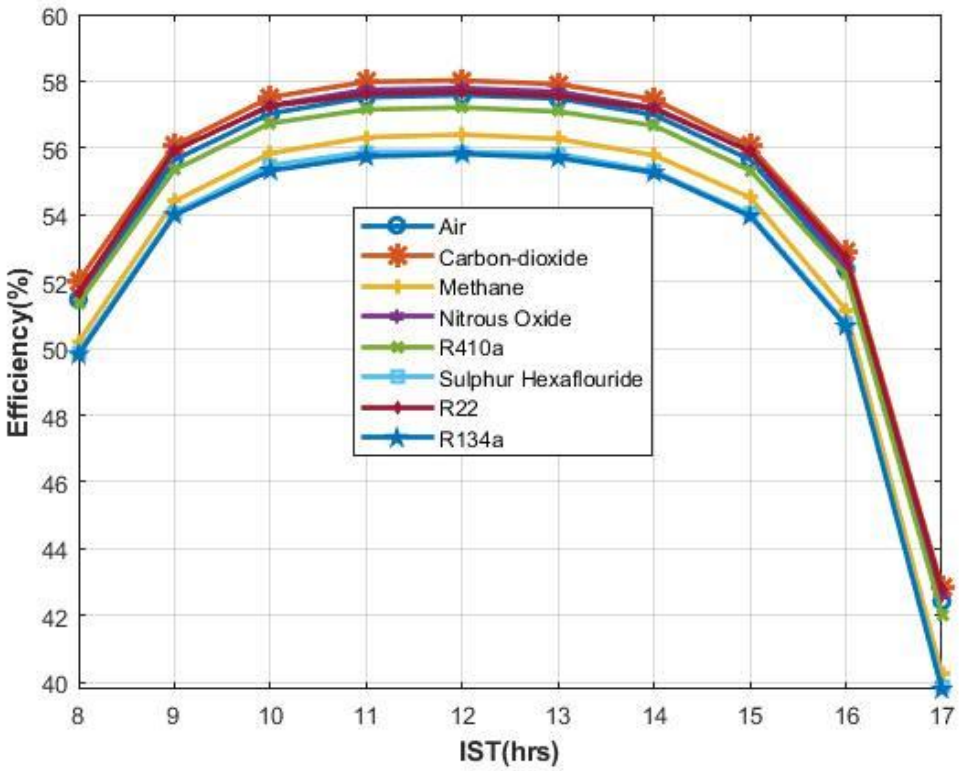

Fig.4.15 Efficiency under hazy and cloudy condition in October

Fig.4.15 shows the variation of instantaneous efficiency over a day under hazy and cloudy condition (17thOctober, 2016). There is 0.85% increase in average efficiency for carbon dioxide filled solar collector and 0.38% and 0.39% increase in average efficiency for nitrous oxide and R22 filled collectors respectively. Other gas filled collectors do not show increase in average efficiency compared to air solar flat plate collector.

4.1.4.4 Cloudy condition

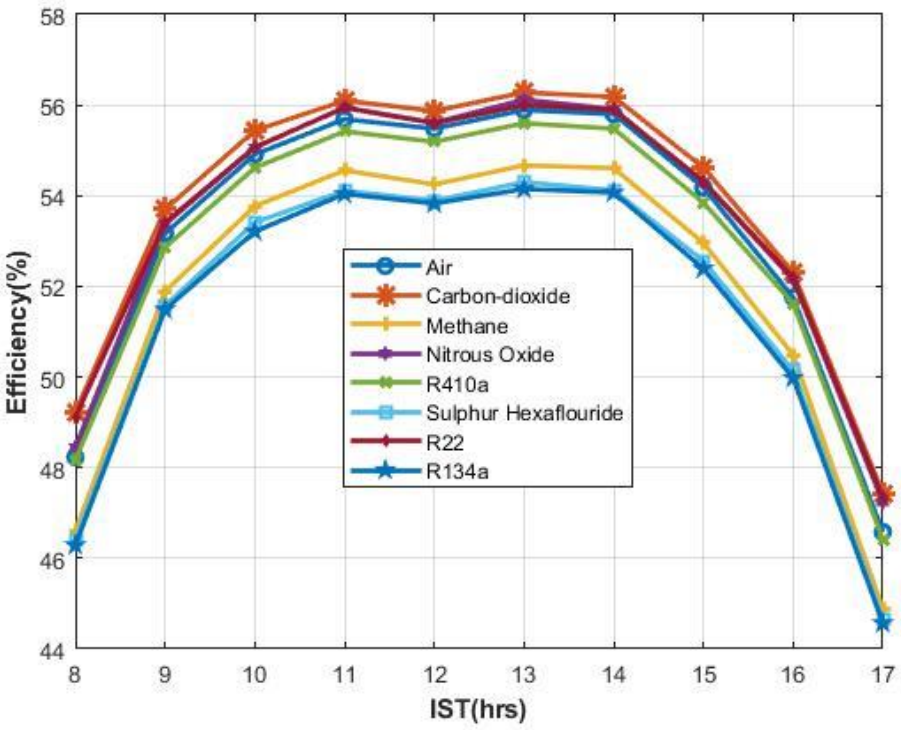

Fig.4.16 Efficiency under cloudy condition in October

Fig.4.16 shows the variation of instantaneous efficiency over a day under cloudy condition (15thOctober, 2016). The carbon dioxide filled collector has increase of 1.03% in average efficiency. Nitrous oxide filled collector shows 0.46% increase and R22 filled one shows 0.60% increase in their efficiency. Other gas filled solar flat plate collector has lower efficiency than air filled solar flat plate collector.

All the above curves are developed with the help of efficiency table calculated with the help of MATLAB codes and has been listed in Appendix 3.

Fig.4.1 to 4.16 shows that there is 0.9% increase in average instantaneous efficiency for carbon dioxide gas,0.41% increase for both nitrous oxides filled and R22 filled solar flat plate collectors compared to air filled solar flat plate collector. This average has been taken over all climatic conditions. All other gas filled collectors are less efficient than air filled solar flat plate collector. The reason for this increase and decreases in efficiency as compared to air filled solar flat plate collector is convective heat transfer coefficient between the absorber plate and glass cover$\left(h_{p-c}\right)$ discussed in section 4.3.

4.2 Overall heat loss coefficient

15 January a clear sky condition has been considered to analyze the overall heat loss coefficient. Table 4.1 and Fig.4.17 shows the variation of overall heat loss coefficient (U_l) for all the gas filled solar flat plate collectors with time for 15 January on hourly basis from 08:00 to 17:00 hrs.

Table 4.1 Variation of overall heat loss coefficient in W/m^2-K of all gases under clear sky condition

Gases	**Indian Standard Time (IST) (hrs)**										
	8	9	10	11	12	13	14	15	16	17	**Average**
Air	4.07	4.24	4.36	4.41	4.44	4.45	4.41	4.36	4.23	4.14	4.31
Carbon dioxide	3.79	3.97	4.09	4.17	4.21	4.22	4.17	4.08	4.01	3.98	4.07
Methane	4.61	4.72	4.88	4.95	4.97	4.99	4.96	4.87	4.75	4.73	4.84
Nitrous Oxide	3.98	4.1	4.21	4.31	4.32	4.33	4.31	4.2	4.09	4.05	4.19
R410a	4.1	4.3	4.49	4.58	4.58	4.62	4.58	4.49	4.36	4.3	4.44
Sulphur hexafluoride	4.66	4.88	4.99	4.96	4.97	4.99	5.06	5.09	4.92	4.8	4.93
R22	3.96	4.1	4.26	4.33	4.36	4.37	4.33	4.26	4.09	4.02	4.21
R134a	4.72	4.98	5.14	5.22	5.23	5.25	5.25	5.16	5.02	4.84	5.08

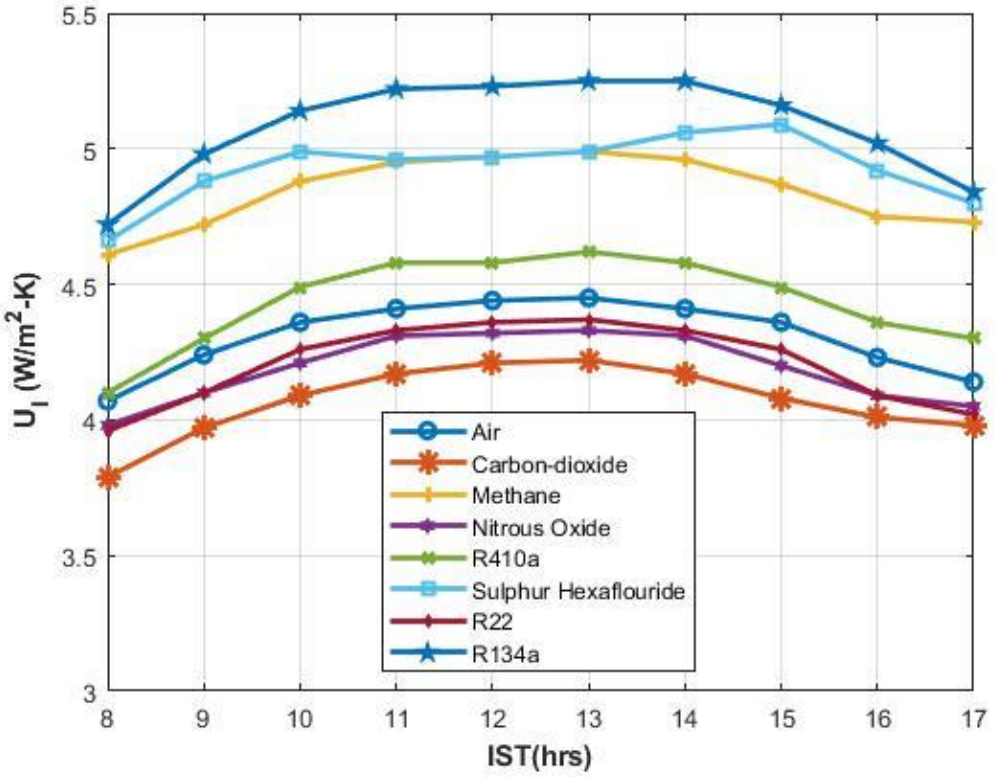

Fig.4.17 Variation of overall heat loss coefficient with IST

It is seen that there is 5.6% decrease in average overall heat loss coefficient for carbon dioxide filled solar flat plate collector as compared to air filled flat plate collector. Also, the nitrous oxide filled collector and R22 filled collector shows 2.8 and 2.3% decrease in average overall heat loss coefficient respectively. Other gas filled collector have increased average overall heat loss coefficient as compared to air filled solar flat plate collector.

4.3 Convective heat transfer coefficient between the absorber plate and glass cover (h_{p-c})

Table 4.2 and Fig.4.18 show the h_{p-c} values for all the gas filled solar flat plate collectors on hourly basis from 08:00 to 17:00hrs for 15 January (clear sky condition).The higher h_{p-c} means the larger amount of heat is lost from the absorber plate to glass through convection. It means that lesser amount of energy is utilized by the working fluid. This convective heat transfer coefficient is the reason behind the

increase and decrease in efficiency of different gas filled solar flat plate collectors compared to the air filled solar flat plate collectors. The gas filled collectors with higher h_{p-c} than air filled solar flat plate collectors have lower efficiency and vice versa.

Also, the gas filled collectors with lower h_{p-c} have lower overall heat loss coefficient, as the top loss coefficient (U_t) is directly dependent on h_{p-c} and U_b and U_s are same for all gas filled solar flat plate collectors.

Table 4.2 Variation of convective heat transfer coefficient between absorber plate and glass cover under clear sky condition

IST (hrs)	**Gases**							
	Air	Carbon dioxide	Methane	Nitrous oxide	R410a	Sulphur hexafluoride	R22	R134a
08:00	2.47	2.17	3.02	2.3	2.51	3.14	2.25	3.22
09:00	2.89	2.56	3.56	2.71	3.02	3.78	2.72	3.87
10:00	3.13	2.81	3.86	2.97	3.31	4.01	3.002	4.26
11:00	3.25	2.93	4.01	3.1	3.46	4.04	3.13	4.41
12:00	3.28	2.97	4.06	3.14	3.51	4.05	3.17	4.42
13:00	3.28	2.97	4.06	3.14	3.51	4.08	3.18	4.46
14:00	3.2	2.9	3.97	3.06	3.43	4.11	3.1	4.4
15:00	3.04	2.73	3.77	2.89	3.23	4.06	2.92	4.14
16:00	2.79	2.49	3.45	2.64	2.92	3.67	2.64	3.75
17:00	2.37	2.1	2.92	2.23	2.41	3.04	2.18	3.12
Average	2.97	2.66	3.66	2.82	3.13	3.79	2.83	4.00

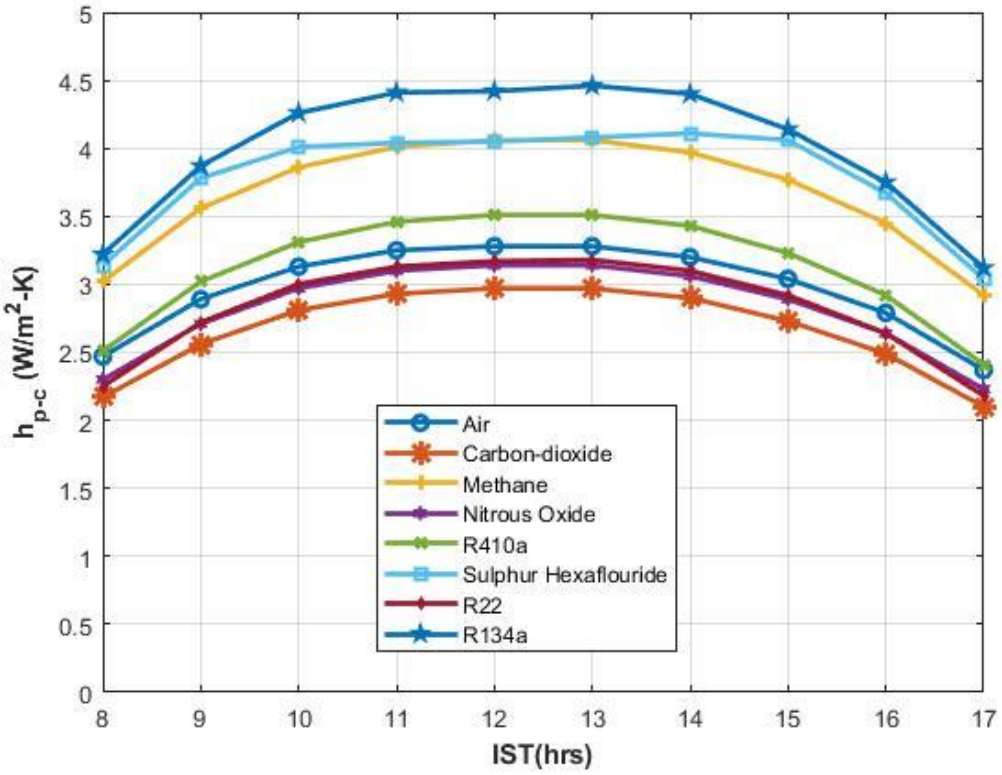

Fig.4.18 Variation of convective heat transfer coefficient between absorber plate and glass cover with IST

It is seen that there is 10.43% decrease in average heat transfer coefficient for carbon dioxide filled solar flat plate collector as compared to air filled solar flat plate collector. Nitrous oxide filled solar flat plate collector shows 5.05% decrease in average heat transfer coefficient and R22 filled solar flat plate collector shows 4.71% decrease in average heat transfer coefficient. Therefore, there efficiencies are greater than air filled solar flat plate collector. All other gas filled collectors have greater average heat transfer coefficient than air filled solar flat plate collector. Therefore, their efficiencies are lower than air filled collector.

4.4 Development of performance characteristic curve and equations

15 January a clear sky condition has been considered for drawing these efficiency curves at 12 noon. The inlet temperature of the water has been varied from ambient temperature i.e. 6.40 to 14.40°C. The horizontal axis is $(T_{fi} - T_a)/I_t$ and the vertical axis show efficiency in percentage. This generally yields straight lines.

4.4.1 Air filled solar flat plate collector

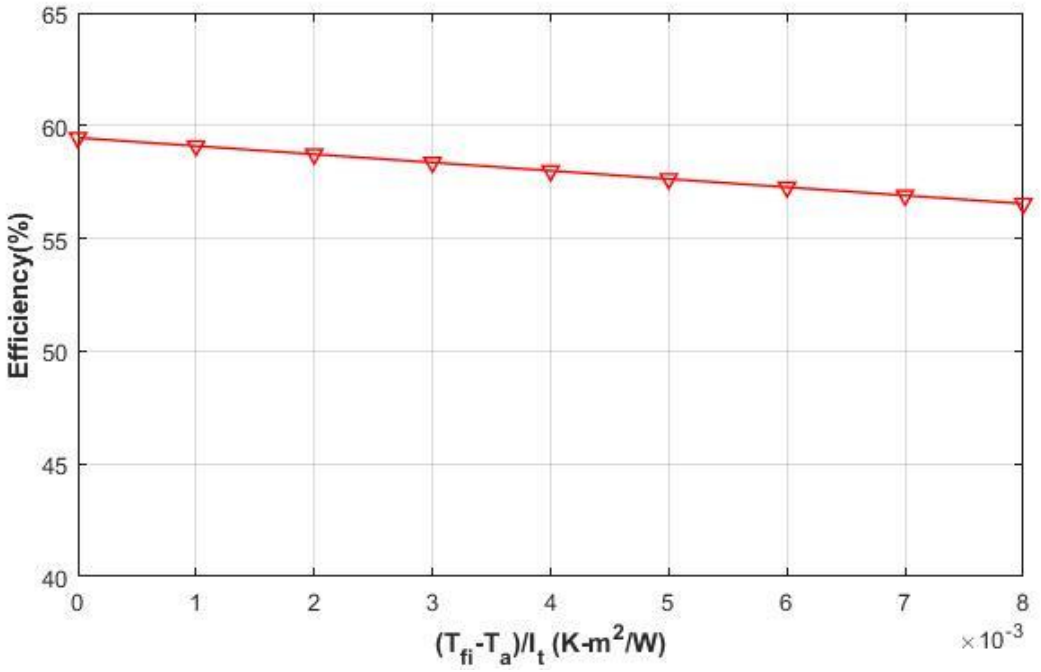

Fig.4.19 Performance characteristic curve for air filled solar flat plate collector

Fig.4.19 shows the performance characteristic curve for air filled solar flat plate collector. Using least square method, we get following equation and it is the characteristic equation for air filled solar flat plate collectors.

$$\eta = 0.595 - 3.653\left(\frac{T_{fi}-T_a}{I_t}\right) \quad (4.1)$$

4.4.2 Carbon dioxide filled solar flat plate collector

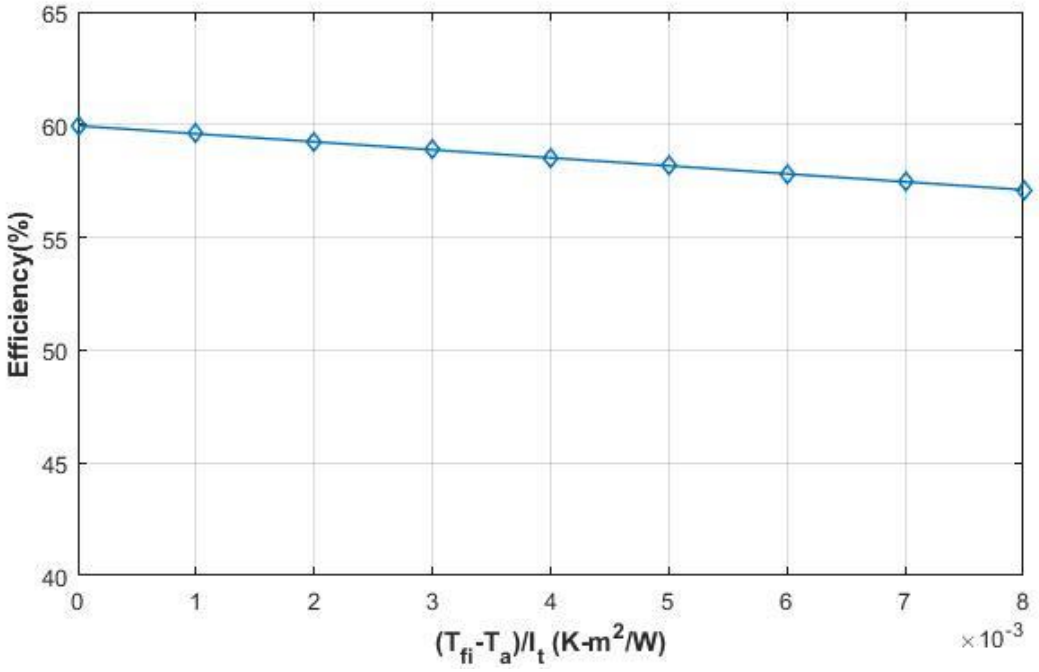

Fig.4.20 Performance characteristic curve for carbon dioxide filled solar flat plate collector

Fig.4.20 shows that performance characteristic curve for carbon dioxide filled solar flat plate collector. The straight-line fitting to this curve i.e. the characteristic equation for carbon dioxide filled solar flat plate collectors is

$$\eta = 0.599 - 3.548\left(\frac{T_{fi}-T_a}{I_t}\right) \quad (4.2)$$

4.4.3 Methane filled solar flat plate collector

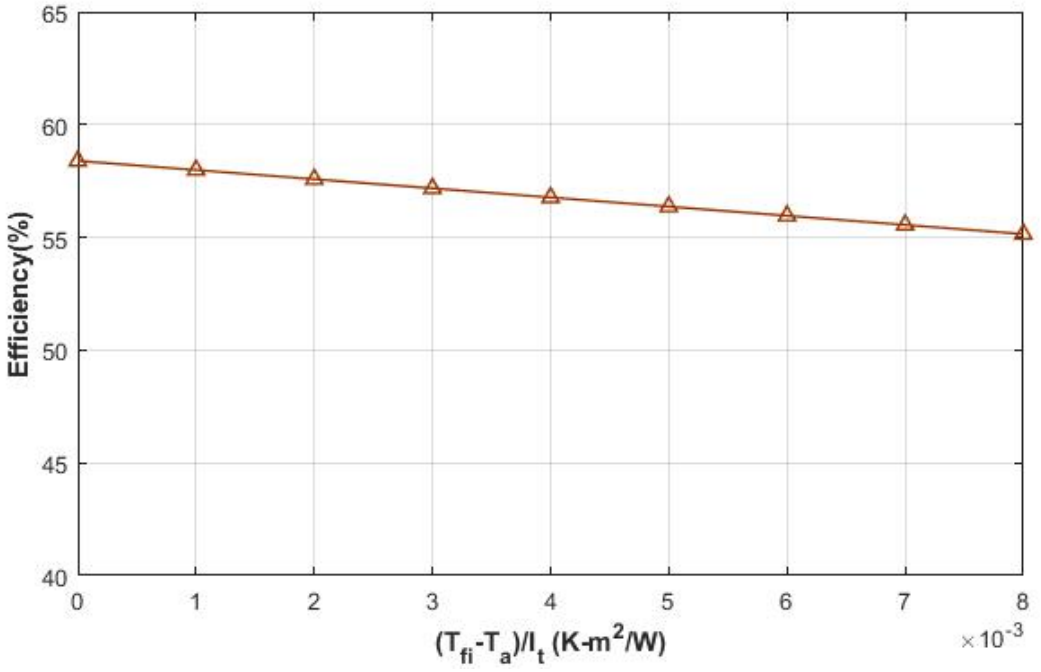

Fig.4.21 Performance characteristic curve for methane filled solar flat plate collector

Fig.4.21 shows the performance characteristic curve for methane filled solar flat plate collector. Using least square method, we get following equation and it is the characteristic equation for methane filled solar flat plate collectors.

$$\eta = 0.584 - 4.057\left(\frac{T_{fi}-T_a}{I_t}\right) \quad (4.3)$$

4.4.4 Nitrous oxide filled solar flat plate collector

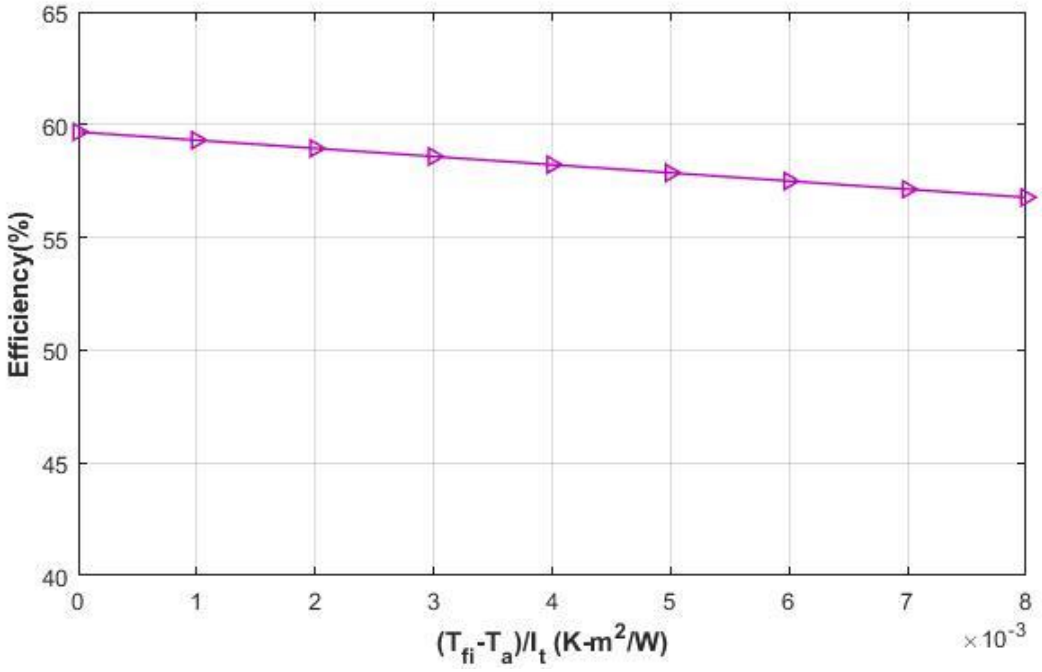

Fig.4.22 Performance characteristic curve for nitrous oxide filled solar flat plate collector

Fig.4.22 shows the performance characteristic curve for nitrous oxide filled solar flat plate collector**.** The straight-line fitting to this curve i.e. the characteristic equation for nitrous oxide filled solar flat plate collector is:

$$\eta = 0.597 - 3.627\left(\frac{T_{fi}-T_a}{I_t}\right) \quad (4.4)$$

4.4.5 R410a filled solar flat plate collector

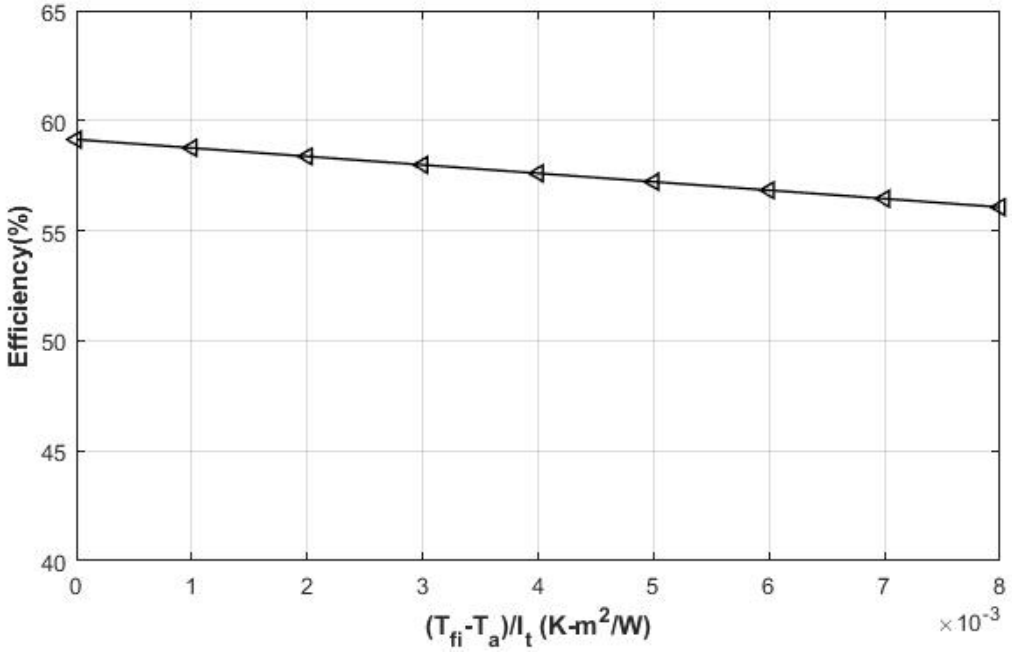

Fig.4.23 Performance characteristic curve for R410a filled solar flat plate collector

Fig.4.23 shows the performance characteristic curve for R410a filled solar flat plate collector**.** Using least square method, we get following equation and it is the characteristic equation for R410a filled solar flat plate collectors.

$$\eta = 0.591 - 3.843\left(\frac{T_{fi}-T_a}{I_t}\right) \qquad (4.5)$$

4.4.6 Sulphur hexafluoride filled solar flat plate collector

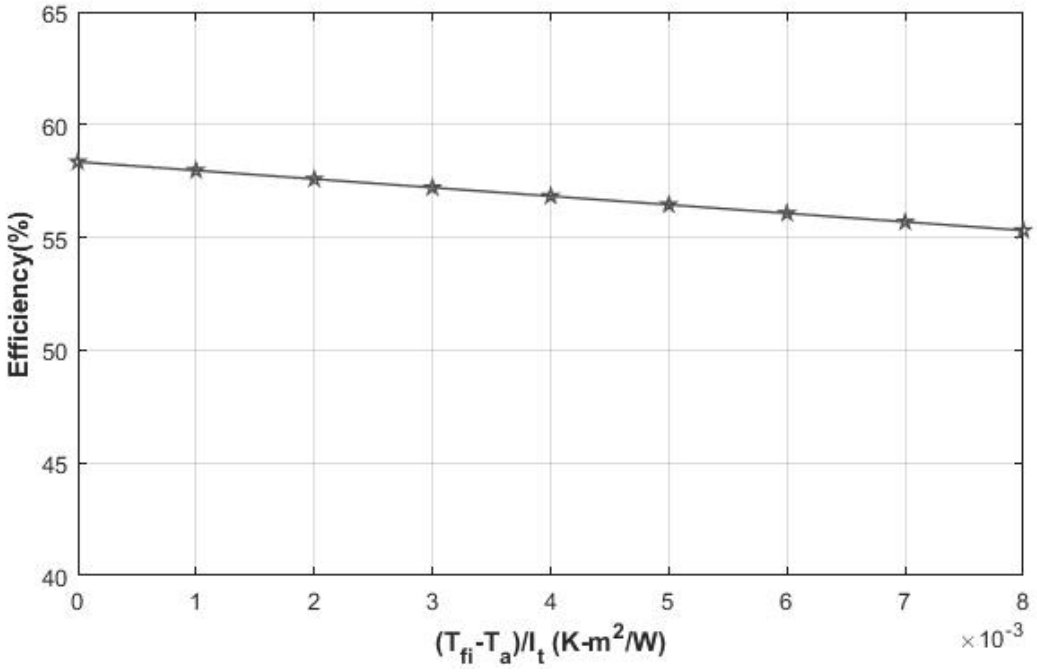

Fig.4.24 Performance characteristic curve for sulphur hexafluoride filled solar flat plate collector

Fig.4.24 shows the performance characteristic curve for sulphur hexafluoride filled solar flat plate collector**.** The straight-line fitting to this curve i.e. the characteristic equation for sulphur hexafluoride filled solar flat plate collectors is

$$\eta = 0.583 - 3.800\left(\frac{T_{fi}-T_a}{I_t}\right) \quad (4.6)$$

4.4.7 R22 filled solar flat plate collector

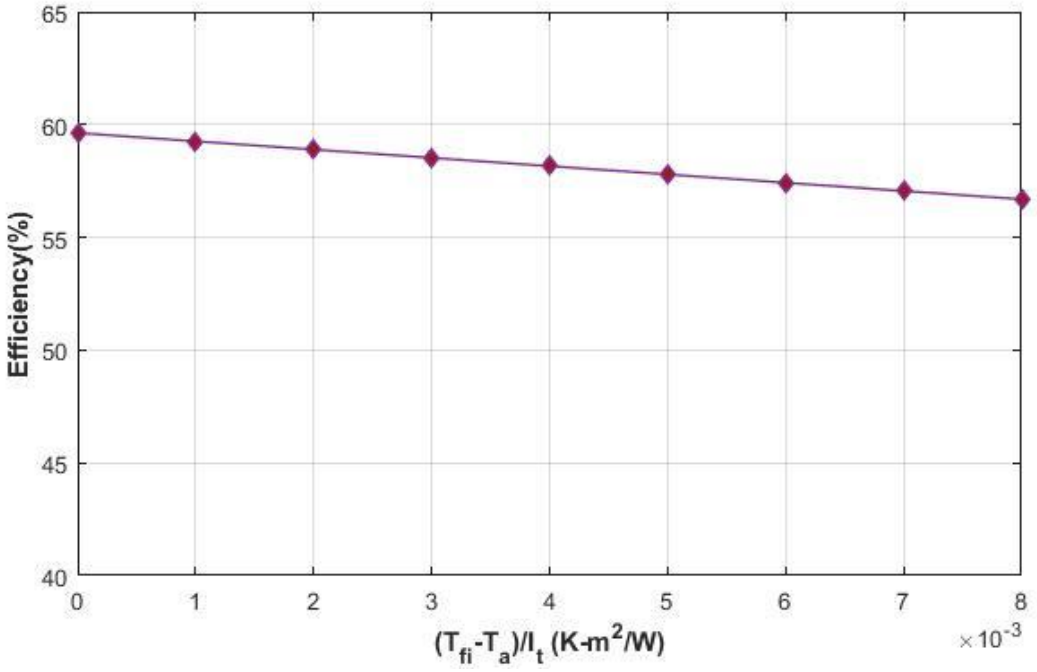

Fig.4.25 Performance characteristic curve for R22 filled solar flat plate collector

Fig.4.25 shows the performance characteristic curve for R22 filled solar flat plate collector**.** Using least square method, we get following equation and it is the characteristic equation for R22 filled solar flat plate collectors.

$$\eta = 0.596 - 3.675\left(\frac{T_{fi}-T_a}{I_t}\right) \quad (4.7)$$

4.4.8 R134a filled solar flat plate collector

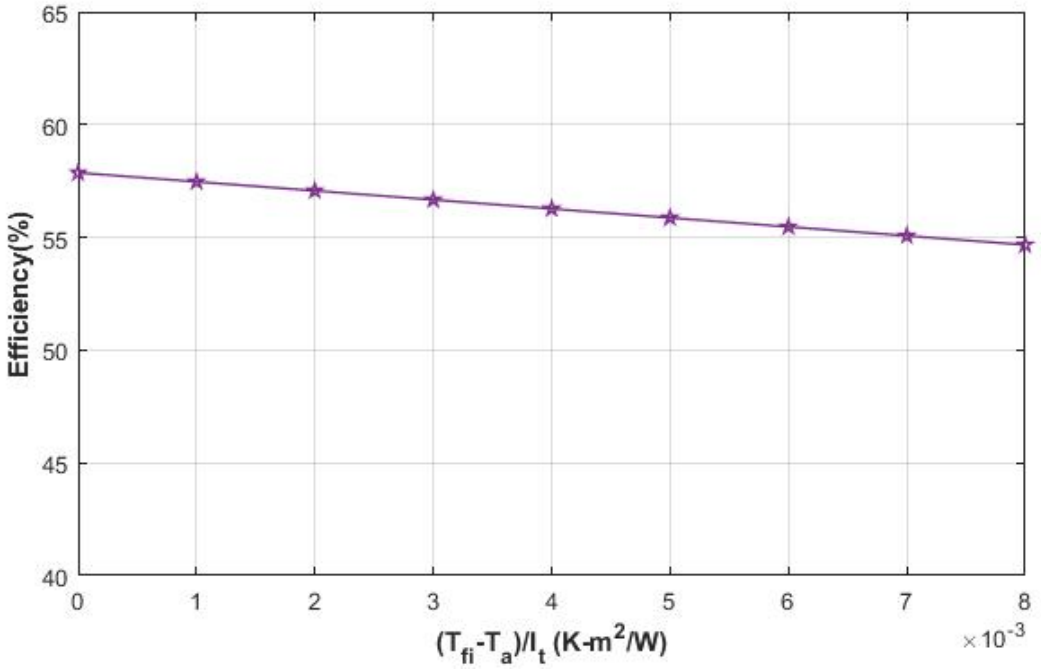

Fig.4.26 Performance characteristic curve for R134a filled solar flat plate collector

Fig.4.26 shows the performance characteristic curve for R134a filled solar flat plate collector**.** The straight-line fitting to this curve i.e. the characteristic equation for R134a filled solar flat plate collectors is

$$\eta = 0.579 - 3.997\left(\frac{T_{fi}-T_a}{I_t}\right) \quad (4.8)$$

Table 4.3 Slope and intercept of characteristic curve for all gas filled solar flat plate collectors

Gases	Slope	Intercept
Air	-3.653	0.595
Carbon dioxide	-3.548	0.599
Methane	-4.057	0.584
Nitrous Oxide	-3.627	0.597
R410a	-3.843	0.591
Sulphur hexafluoride	-3.800	0.583
R22	-3.675	0.596
R134a	-3.997	0.579

Table 4.3 shows that the magnitude of slope for carbon dioxide filled solar flat plate collector is minimum and intercept is maximum. Therefore, the decrease in efficiency of this collector with increase in water inlet temperature is minimum i.e. the performance of carbon dioxide filled solar flat plate collector at higher water inlet temperature is best among all the collectors.

.

CHAPTER 5

CONCLUSIONS & FUTURE SCOPE

5.1 Conclusions

Following conclusions has been drawn on the basis of the present study:

- The average convective heat transfer coefficient between the absorber plate and glass cover decreases about 10.43% for carbon dioxide filled solar flat plate collector, 5.05% for nitrous oxide filled solar flat plate collector and 4.71% for R22 filled solar flat plate collector as compared to air filled solar flat plate collector. Therefore, there efficiencies are greater than air filled solar flat plate collector unlike all other remaining gas filled solar flat plate collectors.
- The carbon dioxide filled solar flat plate collector shows 5.6% decrease in average overall heat loss coefficient. The nitrous oxide filled collector and R22 filled collector show 2.8 and 2.3% decrease in average overall heat loss coefficient as compared to air filled solar flat plate collector respectively. Other gas filled collector have increased average overall heat loss coefficient as compared to air filled solar flat plate collector.
- There is 0.9% increase in average instantaneous efficiency for carbon dioxide gas, 0.41% increase for both nitrous oxide filled and R22 filled solar flat plate collectors as compared to air filled solar flat plate collector.
- The characteristic curve of carbon dioxide filled solar flat collector has the least slope (magnitude) and maximum intercept. It shows that carbon dioxide filled solar flat collector gives the best performance at higher water inlet temperature among all the collectors.

The MATLAB model used in this research can be utilized to analyze any gas filled solar flat plate collector.

5.2 Future scope

- The present research has been conducted by assuming 1 bar pressure inside the solar flat plate collectors. Further investigation can be done to study the influence of pressure on the performance of collectors because these gases have different densities and different amount of gases can be filled inside the spacing at different pressures and corresponding properties of gases will be different.
- Computational fluid dynamics analysis of gas filled solar collector can be done to obtain some detailed results that can be helpful in enhancing the collector's performance.

REFERENCES

[1] Reasons for increase in demand for energy, BBC Bitesize (https://www.bbc.com/bitesize/guides/zpmmmp3/revision/1 accessed on 6 June, 2019)

[2] BP: World Reserves of Fossil Fuels
Published: Monday, July 30 2018, Knoema, (https://knoema.com/infographics/smsfgud/bp-world-reserves-of-fossil-fuels accessed on 5 June, 2019)

[3] What is the Potential of Solar Energy?, Energy Informative

(https://energyinformative.org/potential-of-solar-energy/ accessed on 6 June, 2019)

[4] Kalogirou, S. A. (2004). Solar thermal collectors and applications. *Progress in energy and combustion science*, *30*(3), 231-295

[5] Flat Plate Collector, Alternative Energy Tutorials, Home of alternative and renewable energy tutorials. (http://www.alternative-energy-tutorials.com/solar-hot-water/flat-plate-collector.html accessed on 18 May, 2019)

[6] Iordanou, Grigorios (2009) Flat-Plate Solar Collectors for Water Heating with Improved Heat Transfer for Application in Climatic Conditions of the Mediterranean Region, Durham theses, Durham University. Available at Durham E-Theses Online: http://etheses.dur.ac.uk/174/

[7] Sukhatme S.P and Nayak, J.P. (2008). *Solar Energy, Principles of thermal storage* (3rd ed.). Delhi, McGraw Hill Education

[8] Parabolic Trough Reflector, Alternative Energy Tutorials, Home of alternative and renewable energy tutorials. (http://www.alternative-energy-tutorials.com/solar-hot-water/flat-plate-collector.html accessed on 7 June, 2019)

[9] Treadwell, G. W. (1979). Low-temperature performance comparisons of parabolic-trough and flat-plate collectors based on typical meteorological year data. *NASA STI/Recon Technical Report N*, *79*.

[10] Romero, M., Buck, R., & Pacheco, J. E. (2002). An update on solar central receiver systems, projects, and technologies. *Journal of solar energy engineering*, *124*(2), 98-108.

[11] The greenhouse effect, The National Institute of Water and Atmospheric Research Ltd (NIWA), New Zealand**,** (https://www.niwa.co.nz/our-science/climate/information-and-resources/clivar/greenhouse accessed on 28 May, 2019)

[12] Makhanlall, D., & Jiang, P. (2015). Performance analysis and optimization of a vapor-filled flat-plate solar collector. *Energy Procedia*, *70*, 95-102.

[13] Moss, R., Shire, S., Henshall, P., Arya, F., Eames, P., & Hyde, T. (2018). Performance of evacuated flat plate solar thermal collectors. *Thermal Science and Engineering Progress*, *8*, 296-306

[14] Vestlund, J., Rönnelid, M., & Dalenbäck, J. O. (2009). Thermal performance of gas-filled flat plate solar collectors. *Solar Energy*, *83*(6), 896-904.

[15] Makhanlall, D., Munda, J. L., & Jiang, P. (2013). Entropy generation in a solar collector filled with a radiative participating gas. *Energy*, *60*, 511-516.

[16] Sadeghi, G., Safarzadeh, H., Bahiraei, M., Ameri, M., & Raziani, M. (2019). Comparative study of air and argon gases between cover and absorber coil in a cylindrical solar water heater: An experimental study. *Renewable Energy*, *135*, 426-436

[17] Garcia, R. P., del Rio Oliveira, S., & Scalon, V. L. (2019). Thermal efficiency experimental evaluation of solar flat plate collectors when introducing convective barriers. *Solar Energy*, *182*, 278-285

[18] Nahar, N. M., & Garg, H. P. (1980). Free convection and shading due to gap spacing between an absorber plate and the cover glazing in solar energy flat-plate collectors. *Applied Energy*, *7*(1-3), 129-145

[19**]** Buchberg, H., Catton, I., & Edwards, D. K. (1976). Natural convection in enclosed spaces—a review of application to solar energy collection. *Journal of Heat Transfer*, *98*(2), 182-188.

[20] Beikircher, T., Goldemund, G., & Benz, N. (1996). Gas heat conduction in an evacuated tube solar collector. *Solar energy*, *58*(4-6), 213-217.

[21] Average Weather in Delhi, Weather Spark.

(https://weatherspark.com/y/109174/Average-Weather-in-New-Delhi-India-Year-Round accessed on 4 May, 2019)

[22] Global Warming Potential, United Nations Climate Change,

(https://unfccc.int/process/transparency-and-reporting/greenhouse-gas-data/greenhouse-gas-data-unfccc/global-warming-potentials accessed on 4 December, 2018)

[23] Refrigerants Environmental Data. Ozone Depletion and Global Warming Potential, The Linde Group, (https://www.linde-gas.com/en/legacy/attachment?files=tcm:Ps17-111483,tcm:s17-111483,tcm:17-111483 accessed on 3 June, 2019)

[24] Cooper, P. I. (1969). The absorption of radiation in solar stills. *Solar energy*, *12*(3), 333-346

[25] Lakshmi, P.D. V, Kumar, M.M, Maharshi, D.& Prasad S.D. (2018). Solar power output with optimum tilt angle using MATLAB. *International Research Journal of Engineering and Technology*,*05*, 1131-1139

[26] Iqbal, M. (1983). *An Introduction to Solar Radiation,* Academic Press, Canada

[27] Hottel, H.C and Woertz, BB. (1942). Performance of flat-plate solar-heat collectors.*Trans.ASME*, 64:91

[28] Test, F. L., Lessmann, R. C., & Johary, A. (1981). Heat transfer during wind flow over rectangular bodies in the natural environment. *Journal of Heat Transfer*, *103*(2), 262-267.

APPENDIX 1

Table of the hourly radiation for Delhi provided by IMD Pune

Source: Atheaya, D. (2016). *Performance evaluation of photovoltaic thermal compound parabolic concentrator (PVT-CPC) system*(Doctoral dissertation).

Table A1.1 A- Clear sky condition

Solar Radiation	Month / Time	January	June	August	October
Diffuse(W/m^2)	8am	52.6	123.89	86.62	44.44
	9am	86.28	149.44	100	68.75
	10am	107.29	157.22	155.3	119.45
	11am	121.53	158.89	176.26	137.5
	12pm	126.39	167.78	189.65	147.92
	1pm	136.63	185	201.26	154.17
	2pm	128.3	180.56	197.48	142.36
	3pm	110.94	176.11	172.72	121.53
	4pm	90.28	142.78	128.28	93.06
	5pm	41.84	116.11	93.69	59.72
Beam(W/m^2)	8am	80.38	312.78	246.97	124.31
	9am	269.27	487.78	428.54	295.83
	10am	447.4	645	519.19	445.83
	11am	559.2	756.11	643.94	556.95
	12pm	600.35	783.89	678.53	613.89
	1pm	597.22	761.11	606.57	602.08
	2pm	527.78	702.22	569.19	543.75
	3pm	389.06	589.45	485.36	422.23
	4pm	221.18	468.89	349.5	269.44
	5pm	64.58	303.89	212.12	92.36

Table A1.2 B- Hazy day (fully)

Solar Radiation	Month / Time	January	June	August	October
Diffuse(W/m^2)	8am	52.75	198.33	170	133.17
	9am	102.57	250.83	218.17	187
	10am	123.09	277.08	252.16	212.5
	11am	149.46	297.5	260.67	232.34
	12pm	155.32	300.42	277.66	238
	1pm	161.18	335.41	280.5	232.34
	2pm	155.32	315	252.16	218.17
	3pm	128.94	291.67	232.34	184.17
	4pm	96.71	274.17	218.17	141.67
	5pm	46.88	207.08	178.5	70.83
Beam(W/m^2)	8am	66.83	235	196.89	126.83
	9am	229.94	390.5	333.61	255
	10am	393.17	517.36	461.39	385.5
	11am	500.95	615.39	571.33	461
	12pm	553.43	699.14	603.44	490
	1pm	562.15	661.25	600.61	469.66
	2pm	495.09	597.89	556.73	397.17
	3pm	369.81	517.22	455.22	280.94
	4pm	218.29	361.39	287.39	141.44
	5pm	63.95	208.92	139.28	27.39

Table A1.3 C- Hazy and cloudy (partially)

Solar Radiation	Month / Time	January	June	August	October
Diffuse(W/m^2)	8am	64.16	277.77	239.58	130.56
	9am	146.66	350.7	290.7	172.22
	10am	195.56	378.47	348.2	205.56
	11am	220	416.66	370.55	230.56
	12pm	226.12	434.03	376.95	241.67
	1pm	226.12	423.61	367.36	236.11
	2pm	210.84	402.78	351.39	213.89
	3pm	180.28	385.41	316.25	188.89
	4pm	122.22	347.22	277.92	141.67
	5pm	51.94	246.53	207.64	63.89
Beam(W/m^2)	8am	6.95	80.56	57.92	65.27
	9am	88.89	204.86	199.3	193.34
	10am	164.44	349.31	249.3	290.55
	11am	237.78	400.01	329.45	356.94
	12pm	289.44	399.31	325.56	382.39
	1pm	289.44	437.5	335.15	372.28
	2pm	251.39	361.11	278.61	300.5
	3pm	173.06	303.48	223.75	194.94
	4pm	95.56	191.67	152.08	88.1
	5pm	19.17	86.8	74.86	9.22

Table A1.4 D- Cloudy (fully)

Solar Radiation	Month / Time	January	June	August	October
Diffuse(W/m^2)	8am	48.16	169.56	177.5	107.34
	9am	107.67	251.31	257.38	195.42
	10am	175.66	360.31	340.2	280
	11am	221	405.72	375.71	335.41
	12pm	246.5	454.17	396.41	364.58
	1pm	255	481.42	428.96	332.5
	2pm	240.83	448.11	402.34	282.91
	3pm	187	393.61	346.13	259.58
	4pm	138.83	330.03	266.25	224.58
	5pm	42.5	260.39	162.71	104.78
Beam(W/m^2)	8am	3.03	65.55	30.96	3.5
	9am	32.44	98.8	101.51	42.25
	10am	61.44	94.57	100.49	95.66
	11am	80.77	189.72	154.7	152.7
	12pm	133.42	217.94	176.23	138.86
	1pm	124.92	200.92	159.51	178.61
	2pm	87.89	183.11	159.75	171.97
	3pm	74.36	143.05	149.98	80.3
	4pm	22.84	96.75	82.09	13.08
	5pm	3.3	20.73	32.57	8.97

Table A1.5 Ambient Temperature (T_a) in ^oC.

Time \ Month	January	June	August	October
12am	7.8	32.1	27	24.9
1am	7.3	27.1	25.5	23
2am	6.6	25.2	25.3	21.1
3am	5	24.1	25	21
4am	4	24	24.6	19
5am	5.3	25	24.6	20
6am	6.4	26.9	24	19.5
7am	6.8	26.6	24.1	20.1
8am	7.9	26.5	24.3	21
9am	7.9	26.3	24.3	21
10am	7.9	26.3	24.3	20.5
11am	6.6	26.5	24.3	20.5
12pm	6.4	27.3	24.4	22.7
1pm	7.7	29.9	25.5	25
2pm	10.6	31.4	25.6	28.3
3pm	13	32.2	26	30.5
4pm	15	33.6	26.4	31.6
5pm	16.5	34.3	27.1	32.7
6pm	17	34.2	28.3	34
7pm	15.8	34.2	28	32.3
8pm	14.1	34.1	27.3	30
9pm	12.9	34	27	28.1
10pm	10.2	35	27.5	27.2
11pm	8.2	35	27.2	26

APPENDIX 2

A2.1 Variation of the wind speed (mph)in Delhi for complete year

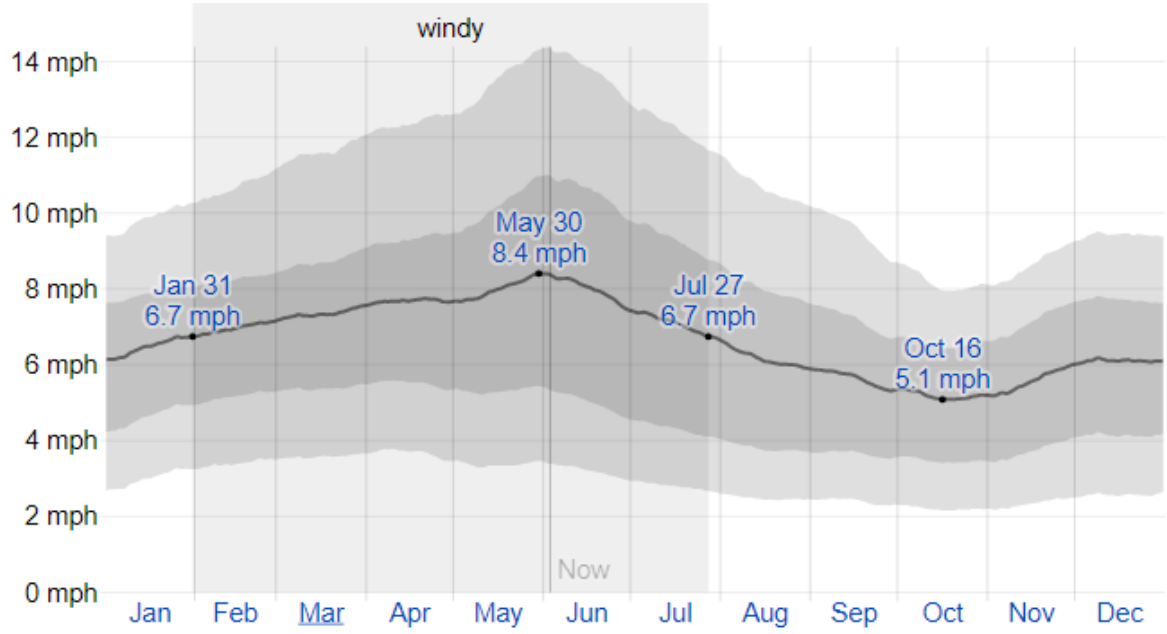

APPENDIX 3

Table A 3.1 15th January- Clear sky condition

Gases	IST (hrs)									
	08:00	09:00	10:00	11:00	12:00	13:00	14:00	15:00	16:00	17:00
Air	47.16	55.32	57.79	58.5	58.75	58.69	58.4	57.61	55.11	46.22
Carbon dioxide	47.76	55.83	58.34	59.05	59.24	59.17	58.9	58.1	55.61	46.82
Methane	46.07	54.24	56.66	57.36	57.58	57.51	57.24	56.42	53.93	45.23
Nitrous Oxide	47.33	55.61	58.02	58.76	58.95	58.88	58.67	57.85	55.39	46.7
R410a	47.12	55.09	57.46	58.17	58.37	58.3	58.05	57.26	54.85	46.15
Sulphur Hexafluoride	45.95	53.93	56.48	57.36	57.6	57.51	57.07	55.99	53.59	45.09
R22	47.33	55.6	57.99	58.73	58.92	58.85	58.57	57.82	55.39	46.82
R134a	45.64	53.74	56.04	56.81	57.06	56.98	56.62	55.91	53.51	44.89

Table A 3.2 17th January- Hazy day (fully)

Gases	IST (hrs)									
	08:00	09:00	10:00	11:00	12:00	13:00	14:00	15:00	16:00	17:00
Air	46.82	55.19	57.65	58.33	58.55	58.5	58.24	57.48	55.13	46.53
Carbon dioxide	47.47	55.78	58.15	58.85	59.05	59.05	58.75	57.98	55.64	47.15
Methane	45.81	54.05	56.48	57.18	57.42	57.37	57.06	56.27	53.94	45.54
Nitrous Oxide	47.3	55.6	57.9	58.55	58.81	58.76	58.45	57.73	55.42	47.02
R410a	46.78	54.95	57.32	58.01	58.22	58.17	57.83	57.12	54.86	46.47
Sulphur Hexafluoride	45.52	53.74	56.25	57.14	57.42	57.3	56.82	55.84	53.8	45.5
R22	47.36	55.6	57.87	58.52	58.72	58.72	58.41	57.69	55.42	47.15
R134a	45.42	53.65	55.92	56.64	56.87	56.81	56.44	55.76	53.52	45.2

Table A 3.3 16th January - Hazy and cloudy (partially)

Gases	IST (hrs)									
	08:00	09:00	10:00	11:00	12:00	13:00	14:00	15:00	16:00	17:00
Air	45.4	54	56.2	57.14	57.52	57.49	57.23	56.33	53.88	44.78
Carbon dioxide	46.02	54.58	56.84	57.64	58.12	58.12	57.79	56.75	54.45	45.24
Methane	43.62	52.9	55.12	56.05	56.39	56.35	56.03	55.09	52.74	43.08
Nitrous Oxide	45.73	54.41	56.6	57.44	57.8	57.86	57.5	56.5	54.33	45.02
R410a	45.42	53.92	55.96	56.9	57.28	57.25	56.97	56.06	53.78	44.74
Sulphur Hexafluoride	43.54	52.68	54.8	55.64	56.1	56.04	55.7	54.75	52.37	42.92
R22	46.02	54.45	56.6	57.43	57.78	57.74	57.49	56.5	54.33	45.14
R134a	43.38	52.46	54.58	55.54	55.89	55.85	55.52	54.67	52.28	42.8

Table A 3.4 18th January - Cloudy (fully)

Gases	IST (hrs)									
	08:00	09:00	10:00	11:00	12:00	13:00	14:00	15:00	16:00	17:00
Air	41.99	52.01	54.36	55.15	56.17	55.95	55.18	54.6	51.82	39.98
Carbon dioxide	42.93	52.45	54.99	55.73	56.68	56.61	55.89	55.07	52.25	40.67
Methane	39.38	50.47	53.21	54.1	54.95	54.85	54.16	53.48	50.33	36.99
Nitrous Oxide	42.4	52.16	54.81	55.44	56.47	56.31	55.6	55.07	52.03	40.33
R410a	42.04	51.96	54.3	55.04	55.93	55.82	55.08	54.51	51.76	39.93
Sulphur Hexafluoride	39.29	50.36	53.06	53.78	54.64	54.54	53.82	53.12	50.18	36.81
R22	42.61	52.34	54.85	55.57	56.47	56.31	55.6	55.07	52.1	40.56
R134a	39.08	50.24	52.87	53.67	54.54	54.31	53.57	53.02	50.08	36.61

Table A 3.5 17th June - Clear sky condition

Gases	IST (hrs)									
	08:00	09:00	10:00	11:00	12:00	13:00	14:00	15:00	16:00	17:00
Air	49.41	55.03	57.07	57.82	57.99	57.84	57.53	56.53	54.01	46.46
Carbon dioxide	49.88	55.55	57.52	58.24	58.39	58.23	57.86	56.97	54.39	46.92
Methane	48.16	53.84	55.87	56.59	56.7	56.54	56.19	55.29	52.76	45.47
Nitrous Oxide	49.53	55.28	57.27	58.01	58.16	58.01	57.62	56.72	54.11	46.78
R410a	49.23	54.71	56.73	57.4	57.56	57.33	57.01	56.08	53.67	46.31
Sulphur Hexafluoride	47.85	53.44	55.37	56.03	56.14	55.97	55.62	54.78	52.36	44.95
R22	49.55	55.26	57.23	57.95	58.1	57.87	57.57	56.68	54.09	46.81
R134a	47.78	53.39	55.24	55.92	56.1	55.87	55.58	54.65	52.2	44.91

Table A 3.6 16thJune - Hazy day (fully)

Gases	IST (hrs)									
	08:00	09:00	10:00	11:00	12:00	13:00	14:00	15:00	16:00	17:00
Air	50.41	54.76	56.42	57.06	57.29	57.05	56.21	55.97	53.78	48.75
Carbon dioxide	50.88	55.15	56.87	57.48	57.75	57.44	56.66	56.39	54.27	49.2
Methane	49.36	53.57	55.14	55.77	56.04	55.79	54.96	54.77	52.58	47.65
Nitrous Oxide	50.73	54.88	56.63	57.25	57.46	57.22	56.41	56.15	54	48.85
R410a	50.27	54.44	56	56.64	56.87	56.56	55.86	55.62	53.45	48.59
Sulphur Hexafluoride	48.96	53.08	54.66	55.22	55.48	55.3	54.45	54.31	52.18	47.23
R22	50.75	54.86	56.49	57.12	57.39	57.08	56.37	56.11	53.99	49.05
R134a	48.79	53.02	54.61	55.17	55.5	55.14	54.41	54.15	52.03	47.19

Table A 3.7 18th June - Hazy and cloudy (partially)

Gases	IST (hrs)									
	08:00	09:00	10:00	11:00	12:00	13:00	14:00	15:00	16:00	17:00
Air	51.73	54.03	55.63	56.04	56.08	56.26	55.79	55.11	53.48	50.45
Carbon dioxide	52.23	54.58	56	56.47	56.51	56.59	56.23	55.57	54.4	50.95
Methane	50.6	52.93	54.41	54.87	54.92	54.94	54.58	53.95	52.34	49.37
Nitrous Oxide	52.08	54.29	55.75	56.23	56.27	56.36	55.98	55.32	53.72	50.8
R410a	51.59	53.85	55.21	55.62	55.75	55.75	55.45	54.77	53.14	50.29
Sulphur Hexafluoride	50.19	52.54	53.93	54.31	54.36	54.45	54.09	53.45	51.81	48.81
R22	52.1	54.28	55.72	56.19	56.23	56.31	55.95	55.29	53.72	50.83
R134a	50.12	52.36	53.79	54.26	54.31	54.34	53.96	53.31	51.76	48.76

Table A 3.8 20th June- Cloudy (fully)

Gases	IST (hrs)									
	08:00	09:00	10:00	11:00	12:00	13:00	14:00	15:00	16:00	17:00
Air	50.26	53.34	54.13	55.08	55.26	55.06	54.82	54.25	53.14	51.56
Carbon dioxide	50.91	53.85	54.57	55.47	55.63	55.42	55.18	54.76	53.57	52.1
Methane	49.17	52.18	52.94	53.88	54.02	53.81	53.64	53.12	51.89	50.41
Nitrous Oxide	50.75	53.47	54.26	55.2	55.37	55.16	55.04	54.49	53.25	51.95
R410a	50.15	53.14	53.8	54.76	54.83	54.62	54.48	53.91	52.9	51.4
Sulphur Hexafluoride	48.84	51.76	52.4	53.38	53.53	53.32	53.13	52.59	51.47	49.91
R22	50.8	53.49	54.26	55.18	55.35	55.13	54.9	54.48	53.4	51.98
R134a	48.77	51.58	52.34	53.33	53.48	53.27	53.09	52.54	51.43	49.75

Table A 3.9 16th August- Clear sky condition

Gases	IST (hrs)									
	08:00	09:00	10:00	11:00	12:00	13:00	14:00	15:00	16:00	17:00
Air	49.15	55.56	57.37	57.96	58.09	57.92	57.73	57.03	54.85	47.81
Carbon dioxide	49.65	56.08	57.83	58.45	58.56	58.34	58.15	57.49	55.27	48.33
Methane	47.86	54.37	56.11	56.79	56.87	56.67	56.45	55.84	53.62	46.68
Nitrous Oxide	49.28	55.8	57.58	58.15	58.26	58.11	57.84	57.25	55.09	48.15
R410a	48.82	55.25	56.97	57.57	57.69	57.53	57.33	56.63	54.54	47.69
Sulphur Hexafluoride	47.67	54	55.64	56.26	56.35	56.14	55.98	55.37	53.24	46.28
R22	49.31	55.79	57.46	58.09	58.21	58.06	57.8	57.21	55.09	48.21
R134a	47.42	53.84	55.58	56.14	56.24	56.09	55.87	55.24	53.18	46.21

Table A 3.10 18th August- Hazy day (fully)

Gases	IST (hrs)									
	08:00	09:00	10:00	11:00	12:00	13:00	14:00	15:00	16:00	17:00
Air	52.37	56.36	57.77	58.31	58.45	57.53	57.46	57.21	55.23	49.72
Carbon dioxide	52.81	56.84	58.19	58.78	58.83	57.99	57.87	57.65	55.75	50.21
Methane	51.46	55.4	56.7	57.21	57.3	56.32	56.21	56.09	54.2	48.6
Nitrous Oxide	52.49	56.59	57.97	58.49	58.62	57.7	57.57	57.41	55.48	49.84
R410a	52.1	56.1	57.5	57.95	58.02	57.14	57	56.92	54.95	49.58
Sulphur Hexafluoride	51.14	54.98	56.28	56.79	56.81	55.8	55.69	55.64	53.74	48.2
R22	52.52	56.59	57.94	58.45	58.5	57.65	57.52	57.38	55.48	49.88
R134a	50.99	54.92	56.23	56.68	56.76	55.75	55.64	55.59	53.68	48.14

Table A 3.11 19th August- Hazy and cloudy (partially)

Gases	IST (hrs)									
	08:00	09:00	10:00	11:00	12:00	13:00	14:00	15:00	16:00	17:00
Air	51.7	54.47	55.58	56.3	56.37	56.42	56.08	55.39	53.92	50.64
Carbon Dioxide	52.28	55.01	56.06	56.74	56.82	56.86	56.45	55.89	54.35	51.17
Methane	50.54	53.27	54.46	55.07	55.15	55.19	54.88	54.22	52.77	49.45
Nitrous Oxide	51.84	54.73	55.8	56.5	56.58	56.62	56.2	55.62	54.19	50.77
R410a	51.53	54.17	55.28	55.91	55.98	56.03	55.68	55.08	53.6	50.46
Sulphur Hexafluoride	50.13	52.91	54	54.62	54.7	54.73	54.42	53.85	52.39	49.03
R22	51.87	54.74	55.78	56.47	56.46	56.5	56.17	55.61	54.2	50.81
R134a	49.95	52.84	53.94	54.56	54.64	54.68	54.28	53.69	52.2	48.96

Table A 3.1220th August Cloudy (fully)

Gases	IST (hrs)									
	08:00	09:00	10:00	11:00	12:00	13:00	14:00	15:00	16:00	17:00
Air	50.83	53.79	54.41	55.18	55.39	55.11	55.05	54.87	53.41	50.12
Carbon dioxide	51.56	54.35	54.84	55.57	55.78	55.59	55.54	55.27	53.73	50.44
Methane	49.63	52.55	53.28	54.01	54.16	53.99	53.91	53.66	52.17	48.66
Nitrous Oxide	50.99	53.92	54.69	55.3	55.52	55.33	55.28	54.99	53.57	50.27
R410a	50.72	53.46	54.1	54.88	54.99	54.81	54.75	54.56	53.1	50
Sulphur Hexafluoride	49.14	52.16	52.78	53.54	53.79	53.52	53.54	53.3	51.78	48.33
R22	51.05	53.94	54.69	55.29	55.5	55.31	55.26	54.99	53.59	50.34
R134a	49.05	52.09	52.72	53.47	53.64	53.47	53.38	53.12	51.71	48.25

Table A 3.13 20th October-Clear sky condition

Gases	IST (hrs)									
	08:00	09:00	10:00	11:00	12:00	13:00	14:00	15:00	16:00	17:00
Air	51.21	56.63	58.05	58.51	58.52	58.39	58.07	57.06	53.56	41.88
Carbon Dioxide	51.54	57.18	58.5	58.92	58.96	58.84	58.45	57.39	54.05	42.39
Methane	49.97	55.56	56.86	57.26	57.3	57.17	56.85	55.83	52.38	40.82
Nitrous Oxide	51.37	56.9	58.26	58.7	58.74	58.56	58.23	57.16	53.78	42.25
R410a	50.85	56.46	57.68	58.07	58.13	57.95	57.67	56.65	53.24	41.76
Sulphur Hexafluoride	49.68	55.09	56.41	56.76	56.8	56.65	56.33	55.29	52	40.39
R22	51.42	56.89	58.22	58.58	58.62	58.5	58.18	57.12	53.77	42.29
R134a	49.47	55.02	56.28	56.7	56.69	56.56	56.23	55.25	51.96	40.34

Table A 3.14 18thOctober- Hazy day (fully)

Gases	IST (hrs)									
	08:00	09:00	10:00	11:00	12:00	13:00	14:00	15:00	16:00	17:00
Air	52.17	56.01	57.4	57.81	57.88	57.78	57.37	56.32	53.07	43.29
Carbon Dioxide	52.66	56.68	57.85	58.3	58.35	58.25	57.78	56.68	53.51	43.61
Methane	50.91	54.88	56.22	56.62	56.7	56.58	56.17	55.08	51.82	41.63
Nitrous Oxide	52.29	56.25	57.61	58.01	58.06	57.96	57.55	56.43	53.18	43.42
R410a	51.84	55.73	57.03	57.44	57.51	57.4	56.97	55.9	52.73	43.01
Sulphur Hexafluoride	50.72	54.43	55.78	56.12	56.2	56.06	55.64	54.6	51.42	40.91
R22	52.32	56.24	57.57	57.96	58.01	57.91	57.51	56.41	53.2	43.52
R134a	50.48	54.36	55.65	56.06	56.09	56.01	55.59	54.55	51.37	40.84

Table A 3.15 17th October- Hazy and cloudy (partially)

Gases	IST (hrs)									
	08:00	09:00	10:00	11:00	12:00	13:00	14:00	15:00	16:00	17:00
Air	51.46	55.64	57.03	57.52	57.58	57.48	56.99	55.65	52.36	42.43
Carbon Dioxide	52.02	56.08	57.52	57.98	58.02	57.91	57.45	56.05	52.87	42.85
Methane	50.19	54.41	55.84	56.32	56.4	56.27	55.78	54.52	51.15	40.24
Nitrous Oxide	51.62	55.92	57.27	57.74	57.79	57.68	57.2	55.9	52.48	42.61
R410a	51.35	55.35	56.74	57.15	57.21	57.09	56.67	55.33	52.21	42.04
Sulphur Hexafluoride	49.89	54.06	55.48	55.88	55.88	55.82	55.31	54.02	50.72	39.89
R22	51.67	55.93	57.25	57.62	57.67	57.56	57.17	55.9	52.72	42.76
R134a	49.81	53.99	55.32	55.74	55.82	55.7	55.26	53.96	50.66	39.79

Table A 3.16 15 October- Cloudy (fully)

Gases	IST (hrs)									
	08:00	09:00	10:00	11:00	12:00	13:00	14:00	15:00	16:00	17:00
Air	48.23	53.17	54.91	55.69	55.48	55.89	55.8	54.18	51.76	46.58
Carbon Dioxide	49.23	53.7	55.44	56.1	55.87	56.28	56.18	54.62	52.31	47.44
Methane	46.6	51.89	53.77	54.56	54.25	54.67	54.61	52.96	50.49	44.89
Nitrous Oxide	48.45	53.37	55.06	55.95	55.61	56.12	55.91	54.3	52.15	47.24
R410a	48.16	52.86	54.62	55.42	55.19	55.6	55.48	53.85	51.62	46.42
Sulphur Hexafluoride	46.4	51.57	53.41	54.11	53.89	54.3	54.12	52.56	50.14	44.65
R22	49.12	53.41	55.07	55.94	55.6	56	55.9	54.32	52.19	47.34
R134a	46.29	51.49	53.21	54.04	53.83	54.15	54.07	52.39	49.98	44.57

APPENDIX 4

List of publications

Mishra, R. K., Meena, P. K., Mishra, R. S., & Pal, A. (2019). Poster presentation on Application of solar energy in the development of Smart cities in India. *Sustainable technologies for environmental management (Stem-2019)* held during 25-26 March, 2019.